

# Final Year Project Report

---

## **Investigation of TR Modulation and Advanced TR Waveform Design**

Mingyu Yang

Teammate: Ye Gu

---

A thesis submitted in part fulfillment of the degree of

**BE.(The Internet of Things Engineering)**

**Supervisor:** Dr. Barry Cardiff



Beijing-Dublin International College

University College Dublin

Beijing University of Technology

May 2017

# **Investigation of Time Reversal Modulation and Advanced TR Waveform Design**

Mingyu Yang

UCD ID: 13205652

May 26, 2017

## Abstract

By focusing signal energy in both time and space domain, Time-reversal(TR) technology provides a great potential of low complexity and energy-efficient communications. With these advantages, TR has become a promising paradigm for future networks such as 5G and Internet of Things(IoT).

In this degree project, we first build up a discrete-time baseband equivalent channel model. To achieve this goal, we start with a simple AWGN channel model to configure the Transmit Filter and Receive Filter. Then, to deal with the multi-path effect, we study the concept of equalization and the FIR realization of two typical linear equalizers(ZFE, MMSE-LE). At last, we focus on channel modeling to achieve better simulation results.

Then, we move on to build up the TR single user model and TR multiple user model. For TR single user model, we only consider the downlink transmission and analyze the average Signal-to-Interference-plus-Noise Ratio(SINR). It is shown that SINR increases when transmit speed declines and path richness grows. As for the multiple user model, both downlink and uplink are analyzed. By measuring the Average Achievable Sum Rate, the tradeoff between transmit speed and user number is explored.

At last, waveform design is discussed to alleviate the performance degradation in high transmit speed, large user density scenarios. For TR single user model, the ideas of pre-equalization and MMSE are applied to suppress the system interference. Both of the ideas can improve the system performance but the latter one has a better performance. Then, the MMSE idea is applied to multiple user model, leading to a huge optimization problem. The solution of this problem is given in this final report and an obvious performance enhancement can be seen.

# Contents

<b>1</b>	<b>Introduction</b>	<b>1</b>
1.1	Motivations of Time-Reversal Modulation . . . . .	1
1.2	Basic Principle of Time-Reversal Modulation . . . . .	2
1.3	Temporal Focusing & Spacial Focusing . . . . .	3
1.4	Literature Review . . . . .	5
1.5	Report Outline . . . . .	7
<b>2</b>	<b>Discrete-time Baseband Equivalent Channel Model</b>	<b>8</b>
2.1	Overview . . . . .	8
2.2	AWGN Channel Model . . . . .	10
2.3	Linear Equalizers . . . . .	11
2.3.1	Basics of Equalization . . . . .	11
2.3.2	Zero Forcing Equalizer . . . . .	12
2.3.3	Minimum Mean Square Error Equalizer . . . . .	15
2.4	Channel Modeling . . . . .	18
2.4.1	Simple channel Model . . . . .	19
2.4.2	802.15.4a Indoor Channel Model . . . . .	20
<b>3</b>	<b>TR Single &amp; Multiple User Model</b>	<b>23</b>
3.1	Overview . . . . .	23
3.2	TR Single User Model . . . . .	23

3.3	TR Multiple User Model . . . . .	26
3.3.1	Downlink For Multiple User Case . . . . .	26
3.3.2	Uplink For Multiple User Case . . . . .	28
<b>4</b>	<b>Waveform Design</b>	<b>31</b>
4.1	Overview . . . . .	31
4.2	Combination of TR system and Equalizers . . . . .	32
4.3	Optimal Waveform Design . . . . .	34
4.3.1	Idea of Waveform Optimization . . . . .	34
4.3.2	Vector Expression of TR System . . . . .	34
4.3.3	Optimal Waveform For Single User Case . . . . .	35
4.3.4	Optimal Waveforms For Multiple User Case . . . . .	37
4.3.5	Concerns With Waveform Optimization . . . . .	43
4.4	Possible Future Work . . . . .	43
<b>5</b>	<b>Conclusion</b>	<b>44</b>
<b>Appendix A. Derivation of MMSE-LE FIR Coefficients</b>		<b>45</b>
<b>Appendix B. Results of KKT Conditions</b>		<b>47</b>

# Chapter 1

## Introduction

### 1.1 Motivations of Time-Reversal Modulation

In recent years, we have witnessed the significant growth of the number of wireless users, along with wide variety of wireless communication applications and services. Moreover, with the appearance of Internet of things(IoT), active things can also be connected to the Internet, leading to a further increase of wireless devices. Such huge amount of wireless devices yields high operational cost and energy consumption, as well as severe interference. To solve this problem, new technologies should be less complex and energy efficient, while guaranteeing good data rate and quality.

As pointed in [1], Time-Reversal(TR) signal transmission is an ideal paradigm for low-complexity, low energy consumption green wireless communication. Its low power consumption comes from its inherent nature to fully harvest energy from the scattering environment by exploiting the multi-path propagation to recollect all the signal energy. Moreover, only one-tap detection is needed at receiver side in TR architecture. As a result, the computational complexity at the terminal devices is low, which means the cost of the terminal devices is also low. However, despite of the reduction in energy and complexity, the achievable rate can still be large given that the bandwidth is wide enough [2]. In addition, the unique location-specific signature in TR system can provide additional physical security, enhancing the privacy and

security of customers.

## 1.2 Basic Principle of Time-Reversal Modulation

The principle of TR transmission is shown in Figure 1.1. Here, the channel is treated as a filter with impulse response  $h(t)$ . When transceiver A wants to transmit information to transceiver B, transceiver B first has to send an impulse-like pilot signal that propagates through a scattering and multi-path environment. The resulting waveforms are received and recorded by transceiver A. This is called channel probing phase. Theoretically, the resulting waveforms are exactly the channel impulse response(CIR). After that, transceiver A simply time-reverses (and conjugated, if the signal is complex) the received waveform and then transmits it back through the same channel to transceiver B. This is called TR-transmission phase. In this phase, the channel behaves as a matched filter for transceiver A.

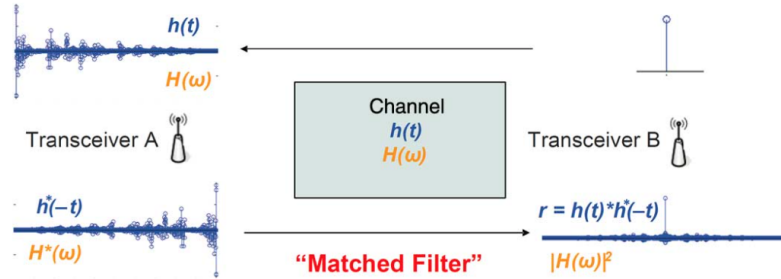


Figure 1.1: Time reversal signal processing principle [1]

To make TR communication system work, three assumptions must be made.

- a) **Perfect knowledge of CIRs:** we assume that after channel probing phase, the CIR is perfectly known at Transceiver A.
- b) **Channel Reciprocity:** the impulse response of the forward link channel and backward link channel are assumed to be identical.
- c) **Channel stationarity:** the CIRs are assumed to be stationary for at least one probing and transmission phase.

The first assumption means that we have perfect channel estimation, which is almost impossible in real wireless communications. However, the current channel estimation technologies are already able to explore most of the channel information. Thus, we just assume that the channel information is well known at Transceiver A for the sake of convenient math derivation. The second assumption guarantees that what Transceiver A gets in channel probing phase is just the forward CIR, and the third assumption means the forward CIR in both phases remains unchanged. The combination of these assumptions makes it possible for us to treat the channel as a matched filter. The last two assumptions generally hold in reality, especially for indoor environment. In [3], Qiu *et al.* conducted experiments in a campus lab area and showed that the correlation between the CIRs of the forward link channel and backward link channel is 0.98, which means the channel is highly reciprocal. In [4], Wang *et al.* conducted experiments and shown that the multi-path channel of an office environment is actually very stationary by measuring the channel information every one minutes and taking 40 channel snapshots in total.

### 1.3 Temporal Focusing & Spacial Focusing

The complexity of TR communication systems is greatly reduced by its temporal focusing and spacial focusing properties. The temporal focusing property of TR comes from the fact that the channel acts as a matched filter in TR transmission phase. In wireless communications, due to the reflection, diffraction and scattering of EM signals, the transmitted signal will arrive at the receiver with different paths. The summation of different signal copies badly distorts the original signal, making the transmission unreliable. To tackle with multi-path effect, several technologies such as orthogonal frequency division multiplexing(OFDM), RAKE receiver and equalization are adopted in wireless communications. In TR transmission, the highest SNR can be achieved in the receiver side. In other words, the signal energy will be concentrated, reducing the inter-symbol interference caused by multi-path effect. Then, in the receiver side, only one-tap detection is required and there is no need for extra techniques. The temporal focusing effect of TR systems is shown in Figure 1.2, taken from [2].

The spacial focusing property of TR stems from the location specificity of reciprocal CIRs.

In TR communication systems, there is a unique CIR between each pair of transceivers. When the re-emitted TR waves from transceiver A propagate in the wireless medium, the location of transceiver B is the only location that is associated with the reciprocal CIR. That is to say that given the re-emitted TR waveform from transceiver A, the environment will serve as a natural matched filter only for the intended location of transceiver B. As a result, the signal energy from other transceivers will be low at transceiver B, introducing little interference. The spacial focusing effect is shown in Figure 1.3 [2]. In this Figure, the spacial focusing effect is valid in wavelength scale.

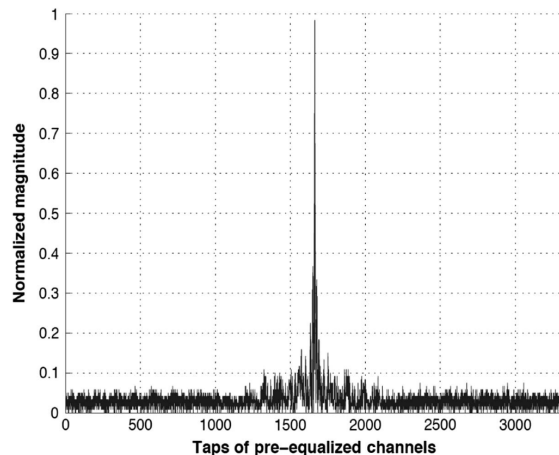


Figure 1.2: Procedure of transmitter mode [2]

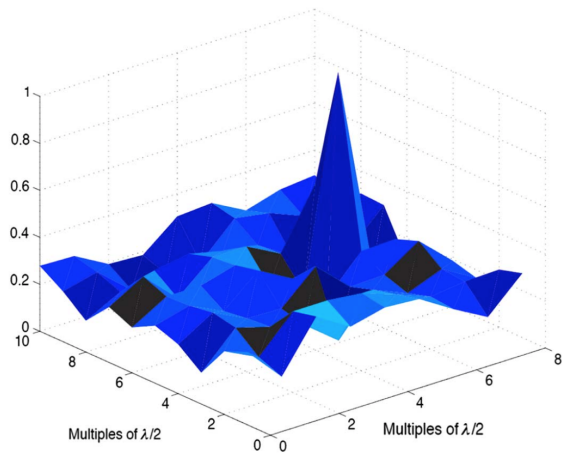


Figure 1.3: Procedure of receiver mode [2]

In the context of communication systems, the temporal focusing effect concentrates a large portion of the useful signal energy of each symbol within a short time interval, which effectively suppresses the inter-symbol interference(ISI) for high-speed broadband communications. The spatial focusing effect allows the signal energy to be harvested at the intended location and reduces leakage to other locations, leading to a reduced transmit power consumption and inter-user interference(IUI) to other locations.

However, time focusing and spacial focusing effect will not eliminate ISI and IUI completely. In some cases, ISI and IUI still limit the system performance. When the symbol rate is very high, the transmitted waveforms will be greatly overlapped, leading to a great ISI and crucial performance degradation as shown in Figure 1.4 and 1.5. Additionally, despite of the inherent

randomness of the CIRs, as long as they are not orthogonal to each other, these waveforms will inevitably interfere with each other. When the number of users is large, the system performance will be greatly impaired by the significant IUI. As a result, our final goal is to design to TR waveform to reduce the effect of ISI and IUI.

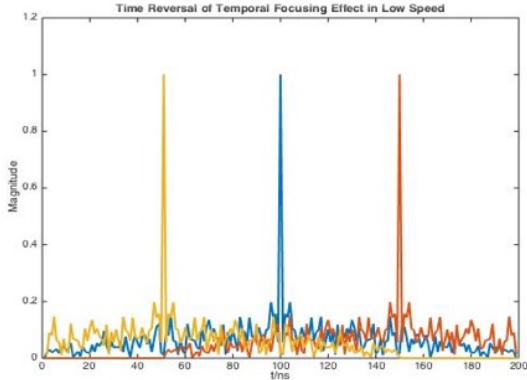


Figure 1.4: Combined channel response in low speed

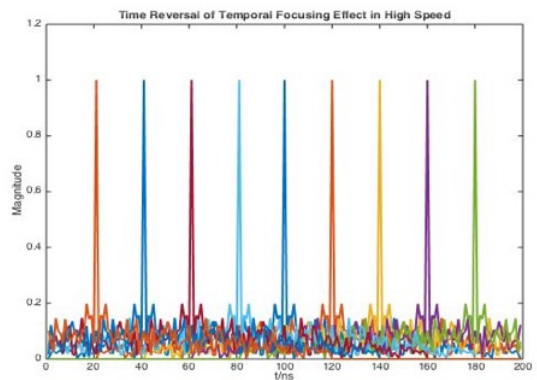


Figure 1.5: Combined channel response in high speed

## 1.4 Literature Review

Time reversal was first applied by M. Fink *et al.* in 1989, where time reversal acoustic mirror (TRM) was used to focus on a reflective target in an inhomogeneous media [5]. As found in his following researches [6, 7], the energy of acoustic waves can be focused at the intended location with a very high resolution, which was then further demonstrated in actual underwater experiments [8, 9] conducted by G. F. Edelmann, T. Akal *et al.*

Due to the special focusing property, TR was then applied to wireless radio communication systems. The first time-reversal experiment was reported for electromagnetic waves in the 2.45 GHz band conducted by Lerosey *et al.* [10]. This suggested that the techniques developed for ultrasound might be used for the electromagnetic case. Other experiments have been conducted in [3, 11–13], including the illustration of temporal and spatial focusing effects.

In wireless communication systems, TR technology were both studied in single-user systems and multi-users systems. In single-user case, the multiple-input/single-output time reversal (MISO-TR) communication system was put forward by Peter Blomgren *et al.* (2008) [14].

They showed that MISO-TR systems caused a rapid loss of coherence in the neighborhood around receivers and led to a highly decreasing BER.

In multi-users system, Gabriel Montaldo, Geoffroy Leroosey *et al.*, found that iterative time reversal performed well in multiple input multiple output multiple users (MIMO-MU) to get lower ISI and lower error rate (2004) [15]. In 2006, H.T.Nguyen *et al.* experimented with 5 users in simultaneous communication to find that the combination of TR systems and ultra-wideband (UWB) technique was an efficient way to support more users and had a better performance in complexity [16].

Feng Han and his team's study (2012) of time-reversal wireless paradigm over multi-path channels represented one of the most advanced ideas that Time-Reversal Division Multiple Access (TRDMA) system performed relatively well in multi-user downlink network. They conducted experiments both in single-antenna and multi-antenna cases using intended-location signatures and found that the progresses on achievable rate region and spatial correlations determines TRDMAs potential for low-complexity energy-efficient broadband wireless communications [17].

Furthermore, Qinyi Xu, Yan Chen, and K. J. Ray Liu (2015) illustrated that in a multiuser communication networks, TR eliminated the IUI effectively while boosting the signal power at the target receiver. This was because of the inherent nature of TR that fully collects energy of multi-path propagation [18].

Most of the recent researches on TR focused on designing better waveform to suppress interference. Yu-Han Yang and K. J. Ray Liu (2016) found out a new waveform design method with interference pre-cancellation by exploiting the message information to further improve the performance in TR systems. Additionally, to solve anti-causal interference (both ISI and IUI) in multi-user waveform design, they proposed two iterative algorithms that one was based on the alternating optimization and the other was a gradient method [19].

## 1.5 Report Outline

The rest of the report is divided into three major parts. In chapter 2, the simulation work of a discrete-time baseband equivalent channel model is introduced. It starts with the simulation of an ideal AWGN channel model. After that, the idea of equalization is discussed, followed by the simulation results of two kinds of linear equalizers. At last, the study of multi-path channel modeling is introduced, and two channel models are simulated afterwards. This chapter aims to build up the standard channel model, which will be used in following TR simulations.

In chapter 3, the simulation work of TR systems is presented. We first focus on the TR single-user case and analyze the system performance. After that, we move further to TR multiple-user case and discuss both downlink and uplink transmissions, followed by their performance analysis.

In chapter 4, we will introduce our work on TR waveform design. First, we attempt to combine TR system with equalizers and the idea of pre-equalization. Then, we focus on optimal waveform designs for both single user case and multiple user case.

Finally, our conclusion is included in chapter 5.

# Chapter 2

## Discrete-time Baseband Equivalent Channel Model

### 2.1 Overview

Our goal in this chapter is to build up a baseband equivalent channel model to support all of our following TR simulations. The model is shown in Figure 2.1. We used a discrete-time baseband equivalent channel because of its convenience in both analysis and simulation work.

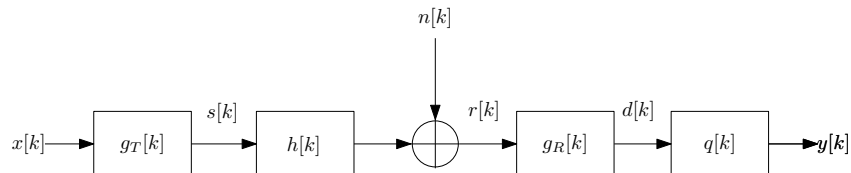


Figure 2.1: Discrete-time baseband equivalent channel model

This channel model contains four main components: Transmit Filter, Receive Filter, Equalizers and Channel. All of them can be realized by FIR filters. The main idea is to make each component modular so that each component is exchangeable.  $x[k]$  is the transmitted symbols and  $y[k]$  is the received symbols.  $n[k]$  is the noise signal, which is assumed to be additive white Gaussian noise(AWGN) in our model. In other words,  $n[k] \sim N(0, N_0B)$ . Since it is baseband equivalent, all the signals and FIR filters are expressed by complex numbers. Also, there is no RF component included in this model because of this baseband equivalent property. The

detailed introduction of these four components is listed below:

- **Transmit Filter( $g_T[k]$ ):** The transmit filter is a FIR filter that shapes the transmitted symbols. It may or may not be a root-Nyquist filter. Before TR simulations, a root-raised-cosine(RRC) filter(one kind of root-Nyquist filter) is adopted as the transmit filter. In contrast, later in the TR simulations, the transmit filter is the time-reversed and conjugated version of CIR.
- **Receive Filter( $g_R[k]$ ):** The transmit filter and receive filter are usually a pair of root-Nyquist filters to reduce ISI. Before TR simulations, the receive filter is RRC filter. However, in TR communications, there is no need of receive filter because of its one-tap detection property.
- **Equalizer( $q[k]$ ):** Many practical channels are bandlimited and linearly distort the transmit signal. In this case, the resulting ISI channel has to be equalized for reliable detection. In this project, only linear equalizers are considered, which can be realized by simple FIR filters.
- **Channel( $h[k]$ ):** In discrete-time channel model,  $h[k]$  can be treated as the channel impulse response. In general, the channel is not ideal, in other words,  $H[z]$  is not a constant over the range of frequencies. In this project, our focus is multi-path channel where each non-zero  $h[k]$  represents one path of the transmitted signal.

The process of building this channel model can be divided into three steps. First, an ideal AWGN channel model is built with Transmit Filter, Receive Filter components. After that, linear equalization is discussed to deal with the Equalizer component. Finally, channel modeling process is discussed to tackle with the Channel component.

## 2.2 AWGN Channel Model

The goal of building up an AWGN channel model is to combine the Transmit Filter and Receive Filter components. After that, the Equalizer and Channel can be integrated with this channel. When the simulation results of AWGN channel model meet with the theory, this model is proved valid. The AWGN channel model is shown in Figure 2.2:

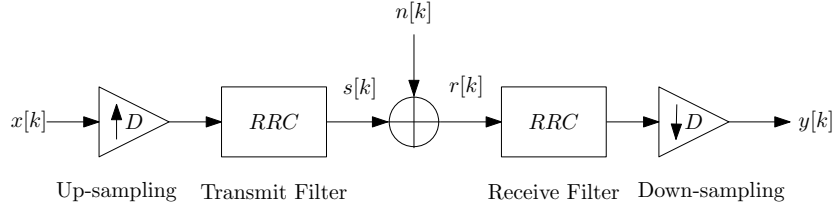


Figure 2.2: Ideal AWGN channel model

Here, two root-raised-cosine(RRC) filters are used as Transmit filter and Receive filter. According to the property of RRC filters, the whole transmit process is ISI-free. Up-sampling and down-sampling are applied here to guarantee the Nyquist frequency. Throughout this section, we adopt linear memoryless modulations such as BPSK, QPSK, and 16QAM for test. The received signal  $y[k]$  can be expressed as:

$$\begin{aligned} y[k] &= x[k] * RRC[k] * RRC[k] + n[k] * RRC[k] \\ &= x[k] * RC[k] + n'[k] \end{aligned}$$

where  $n'[k]$  is colored additive Gaussian noise after RRC filter. However, since RRC filter is a root-Nyquist filter, the PSD of  $n[k]$  will not be changed after RRC filter. As a result,  $n'[k]$  can just be treated as  $n[k]$ . Then the expression becomes  $y[k] = x[k] + n[k]$ , which is a typical AWGN channel. The symbol error rate(SER) during simulations should be the same as their theoretical SERs. The scatter plots of BPSK, QPSK and 16QAM are shown in Figure 2.3, 2.4 and 2.5.

The constellation can be easily recognized in the scatter plots. After that, the SER of each modulation scheme is calculated, as shown in Figure 2.6. It is obvious that the simulation results are almost the same as the theoretical curves. Up to now, it is fair to say that our

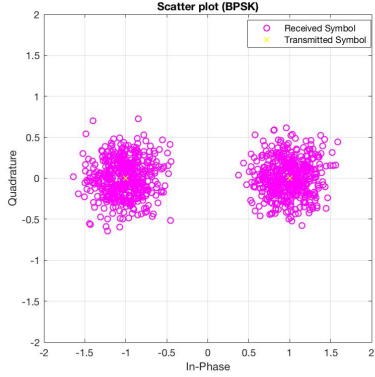


Figure 2.3: Scatter plot (BPSK, Es/N0=10dB)

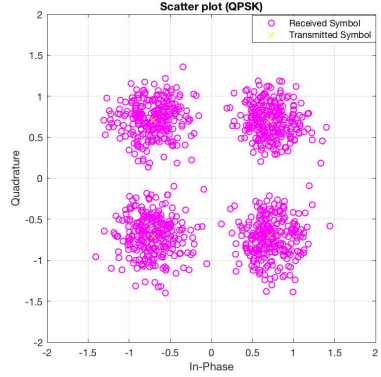


Figure 2.4: Scatter plot (QPSK, Es/N0=10dB)

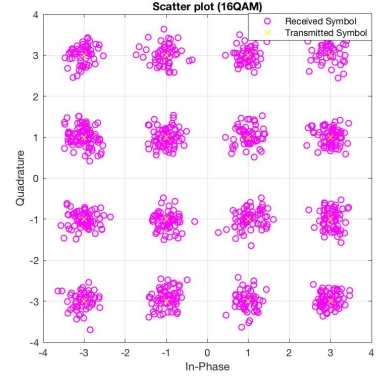


Figure 2.5: Scatter plot (16QAM, Es/N0=20dB)

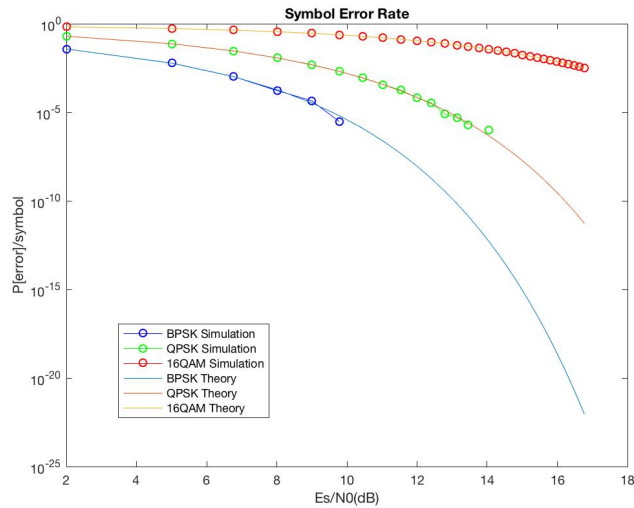


Figure 2.6: SER of simulation and theory

AWGN channel model is configured properly.

## 2.3 Linear Equalizers

### 2.3.1 Basics of Equalization

As is introduced in section 2.1, equalizers are used to eliminate the ISI caused by multi-path propagation. The idea of equalization is that by adding equalizers to the receivers, a new AWGN-like channel can be synthesized at the receiver side. Then, we can analyze the equalized channel using the same method as before. However, the optimum equalizer, maximum-likelihood estimator, is so difficult to realize that in reality some alternative sub-optimal cost-effective equalizers are used to reduce ISI.

In this section, our focus is on linear equalizers(LE), which is the simplest sub-optimal equalizer. LEs can be realized by linear filters such as FIR and IIR filters. However, because of the better stability of FIR than IIR, we focus on FIR realizations of LEs. To better analyze their performance, we simplify the channel model in section 2.1 which is shown in Figure 2.7. In this simplified model, we integrate the Transmit Filter, Receive Filter and Channel into one component called Channel Transfer Response(CTR), which can be expressed as  $h_{ct}[k] = g_T[k] * h[k] * g_R[k]$ . The noise here is again colored noise and  $n'[k] = n[k] * g_R[k]$ . In this model, we assume the Transmit Filter and Receive Filter to be RRC filters. Then, the colored noise  $n'[k]$  can be treated as AWGN just as before. Moreover, we define an overall channel transfer response(OCTR) to further combine CTR and equalizers,  $h_{ov}[k] = h_{ct}[k] * q[k]$ .

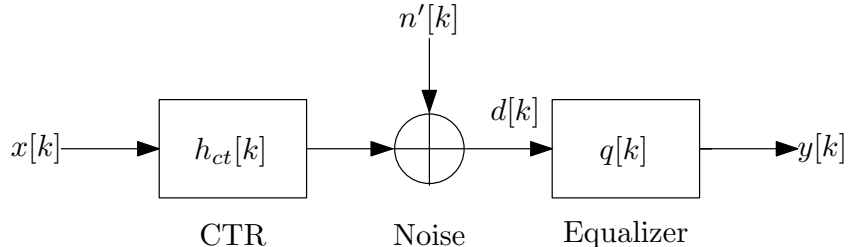


Figure 2.7: Simplified channel model for equalization

In this section, two linear equalizers are discussed. The first one is called zero-forcing equalizers(ZFE), the other is called minimum mean square error linear equalizer(MMSE-LE). Their performance analysis and FIR realizations are discussed in the following sections.

### 2.3.2 Zero Forcing Equalizer

#### Optimum Zero Forcing Equalizer

Zero forcing means that it is our aim to force the residual inter-symbol interference in the decision variable  $d[k]$  to zero. The above goal can be achieved by

$$Q[z] = \frac{1}{H_{ct}[z]}$$

where  $Q[z]$  and  $H_{ct}[z]$  are the z-transform of  $q[k]$  and  $h_{ct}[k]$ .

Since in most practical applications  $H_{ct}[z]$  can be modeled as a filter with FIR,  $Q[z]$  will be an IIR filter in general. Then, to analyze the performance of ZFE, we assume  $Q[z]$  to be IIR first. Obviously, the resulting z-transform of OCTR is

$$H_{ov}[z] = H_{ct}[z]Q[z] = 1 \quad (2.1)$$

Then, the channel is very similar with an AWGN channel and the received signal  $y[k]$  is:

$$y[k] = x[k] + n''[k]$$

where  $n''[k] = n'[k] * q[k]$  is colored Gaussian noise with power spectral density

$$\begin{aligned} S(e^{j2\pi fT}) &= N_0 |Q(e^{j2\pi fT})|^2 \\ &= \frac{N_0}{|H_{ct}(e^{j2\pi fT})|^2} \end{aligned}$$

The corresponding error variance can then be calculated as

$$\begin{aligned} \sigma_e^2 &= \varepsilon |e[k]|^2 \\ &= T \int_{-1/2T}^{1/2T} S(e^{j2\pi fT}) df \\ &= T \int_{-1/2T}^{1/2T} \frac{N_0}{|H_{ct}(e^{j2\pi fT})|^2} df \end{aligned} \quad (2.2)$$

From equation 2.2, we can see that ZFE faces severe performance degradation when  $H_{ct}[z]$  has zeros close to the unit circle. In this case,  $\sigma_e^2 \rightarrow \infty$ . That means the power of error is so large that SNR is nearly 0, which is not acceptable in real wireless communications.

### FIR Realization of ZFE

In this case, we impose a causality and a length constraint on the equalizer filter. The length of equalizer is assumed to be  $N + 1$ . To get the FIR coefficients, we start from its time domain

expression, which can be easily derived from equation 2.1.

$$h_{ov}[k] = \sum_{m=0}^N q[m]h_{ct}[k-m] = \begin{cases} 1 & k = k_0, \\ 0 & elsewhere. \end{cases}$$

where  $k \in \{k_0 - N/2, \dots, k_0 - 1, k_0, k_0 + 1, \dots, k_0 + N/2\}$  and  $k_0$  is the decision delay, i.e., at time  $k$ , we estimate  $x[kk_0]$ . Here, we assume a fixed value for  $k_0$ , but in practice,  $k_0$  can be used for optimization. It can be interpreted that the convolution of  $q[k]$  and  $h_{ct}[k]$  is a delta function. Then, we can write it into a vector form and the coefficients of ZFE filter can then be calculated by

$$\mathbf{q} = \mathbf{H}^{-1}\boldsymbol{\delta}$$

where each component can be expressed as

$$\mathbf{H} = \begin{bmatrix} h_{ct}[k_0] & h_{ct}[k_0 - 1] & \cdots & h_{ct}[k_0 - N] \\ h_{ct}[k_0 + 1] & h_{ct}[k_0] & \cdots & h_{ct}[k_0 - N + 1] \\ \vdots & \vdots & \ddots & \vdots \\ h_{ct}[k_0 + N] & h_{ct}[k_0 + N - 1] & \cdots & h_{ct}[k_0] \end{bmatrix}, \mathbf{q} = \begin{bmatrix} q[0] \\ q[1] \\ \vdots \\ q[N] \end{bmatrix}, \boldsymbol{\delta} = \begin{bmatrix} 0 \\ \vdots \\ 1 \\ \vdots \\ 0 \end{bmatrix}$$

However, for FIR realization of ZFE, we can only guarantee a local delta function in  $N + 1$  successive elements of  $h_{ov}[k]$ . Out of that range, we don't know what values  $h_{ov}[k]$  will be. Note that there is no restriction imposed on the remaining coefficients of  $h_{ov}[k]$  (don't care positions). The don't care positions may take on large values. The simulation results of ZFE in both time domain and frequency domain are shown in Figure 2.8 and 2.9.

In time domain plot, the problem of "don't care positions" is obvious. We can only guarantee an ideal delta function for only 51 samples. Out of that range, there is one  $h_{ov}[k]$  rushing to nearly 0.4, which is extremely large and will cause interference to other symbols. In frequency domain plot, the frequency response of CTR, ZFE coefficients and OCTF are all plotted. It can

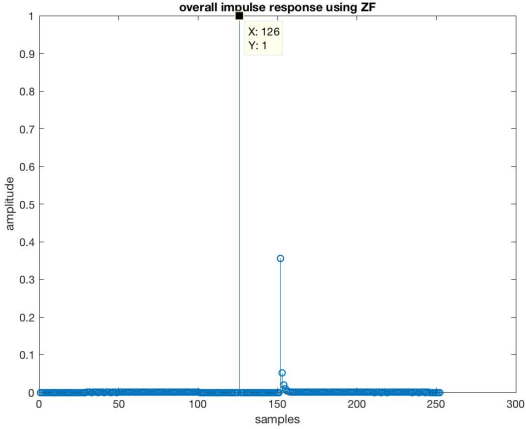


Figure 2.8: Time domain plot of ZFE( $N=50$ )

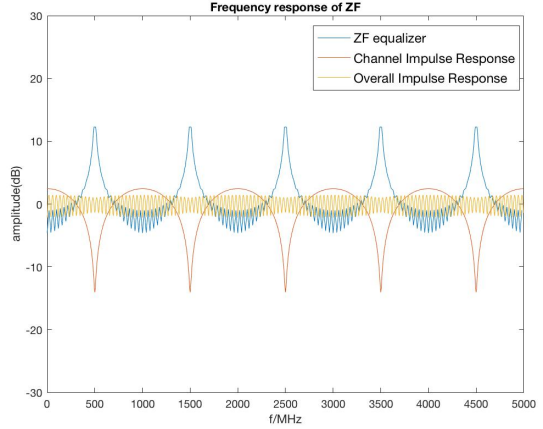


Figure 2.9: Frequency domain plot of ZFE( $N=50$ )

be seen that the plot of OCTF is nearly one but with some fluctuation. That is also because of the finite length delta function resulting from the FIR realization. Besides, the noise problem is also obvious. When the frequency response of CTR reaches the bottom, the frequency response of ZFE reaches its maximum value over 10dB. In this case, large portion of the noise energy will be filtered into the receiver and damage the received signals.

### 2.3.3 Minimum Mean Square Error Equalizer

Unlike ZFE, MMSE-LE does take the noise power into account and aims to minimize the variance of the error signal. The MMSE criterion ensures an optimum tradeoff between residual ISI in  $d[k]$  and noise enhancement. Therefore, MMSE-LE achieve a significantly lower BER compared to ZF equalizers at low-to-moderate SNRs. MMSE-LE can also be realized by FIR. However, the calculation of MMSE-LE coefficients is more difficult. First, we define our error signal to be:

$$e[k] = y[k] - x[k - k_0]$$

After that, the received signal is expressed in a vector form for the convenience of following derivations. Here, the length of MMSE-LE is  $N + 1$ .

$$\begin{aligned} y[k] &= \sum_{m=0}^N q[m]d[k - m] \\ &= \mathbf{q}\mathbf{d}^T = \mathbf{d}\mathbf{q}^T \end{aligned}$$

where  $\mathbf{q} = [q[0], q[1], \dots, q[N]]$ ,  $\mathbf{d} = [d[k], d[k-1], \dots, d[k-N]]$ . Then, the cost function for filter optimization is given by

$$\begin{aligned}
J(\mathbf{q}) &= \varepsilon\{|e[k]|^2\} \\
&= \varepsilon\{e[k]e^*[k]\} \\
&= \varepsilon\{(\mathbf{q}\mathbf{d}^T - x[k-k_0])(\mathbf{d}\mathbf{q}^T - x[k-k_0])^*\} \\
&= \mathbf{q}\varepsilon\{\mathbf{d}^T\mathbf{d}^*\}\mathbf{q}^H - \mathbf{q}\varepsilon\{\mathbf{d}^Tx^*[k-k_0]\} - \varepsilon\{\mathbf{d}^Tx[k-k_0]\}\mathbf{q}^H + \varepsilon\{x[k-k_0]x^*[k-k_0]\} \\
&= \mathbf{q}\Phi_{dd}\mathbf{q}^H - \mathbf{q}\varphi_{dx} - \varphi_{dx}^H\mathbf{q}^H + P_s
\end{aligned} \tag{2.3}$$

where  $\Phi_{dd}$  denotes the autocorrelation matrix of vector  $\mathbf{d}$ , and  $\varphi_{dx}$  is the cross-correlation vector between  $\mathbf{d}$  and  $x[k-k_0]$ .  $\Phi_{dd}$  and  $\varphi_{dx}$  are given by

$$\Phi_{dd} = \begin{bmatrix} \phi_{dd}[0] & \phi_{dd}[1] & \cdots & \phi_{dd}[N] \\ \phi_{dd}[-1] & \phi_{dd}[0] & \cdots & \phi_{dd}[N-1] \\ \vdots & \vdots & \ddots & \vdots \\ \phi_{dd}[-N] & \phi_{dd}[-N+1] & \cdots & \phi_{dd}[0] \end{bmatrix}, \varphi_{dx} = \begin{bmatrix} \phi_{dx}[k_0] \\ \phi_{dx}[k_0-1] \\ \vdots \\ \phi_{dx}[k_0-N] \end{bmatrix}$$

where  $\phi_{dd}[\lambda] = \frac{\sigma^2}{T}h_{ct}[\lambda]*h_{ct}^*[-\lambda] + \frac{N_0}{2}\delta[\lambda]$  and  $\phi_{dx}[\lambda] = \frac{\sigma^2}{T}h_{ct}[k_0+\lambda]$ . The proof of them is left in Appendix A.  $\sigma^2$  is the variance of symbols and  $T$  is the symbol duration.

After that, to get the optimum filter coefficient vector, we need to set the gradient of  $J(\mathbf{q})$  equal to zero. For calculation of this gradient, it is also included in Appendix A, together with the rules for differentiation of scalar functions. Then, we have

$$\begin{aligned}
\frac{\partial J(\mathbf{q})}{\partial \mathbf{q}} &= \Phi_{dd}\mathbf{q}^H - \varphi_{dx} = 0 \\
\mathbf{q} &= (\Phi_{dd}^{-1}\varphi_{dx})^H
\end{aligned} \tag{2.4}$$

After that, the same simulations are conducted on MMSE-LE and the simulation results are shown in Figure 2.10 to 2.13. Since MMSE-LE does consider the noise power, two simulations

with different SNR situations are provided.

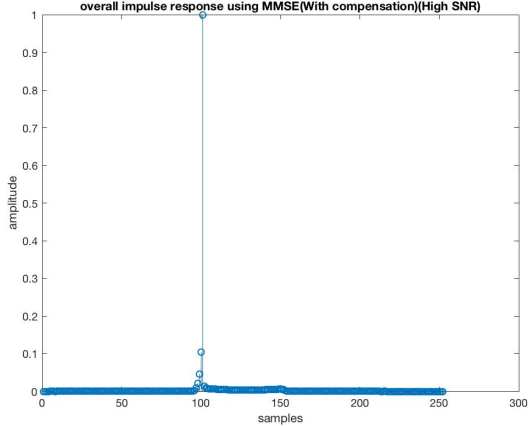


Figure 2.10: Time domain plot of MMSE-LE(N=50, SNR=100)

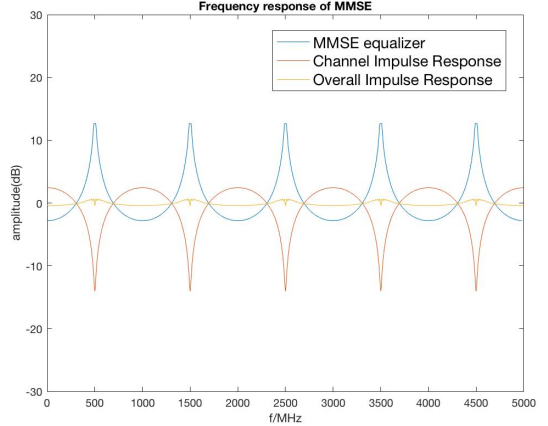


Figure 2.11: Frequency domain plot of MMSE-LE(N=50, SNR=100)

For high SNR scenarios shown in Figure 2.10 and 2.11, the results are very similar with that of ZFE, especially in frequency domain. This similarity makes sense because the noise power is trivial and can thus be ignored. However, in time domain, there is no problem of "don't care positions" because MMSE-LE has constraint on each coefficient. As a result, the resulting OCTF is almost an ideal delta function.

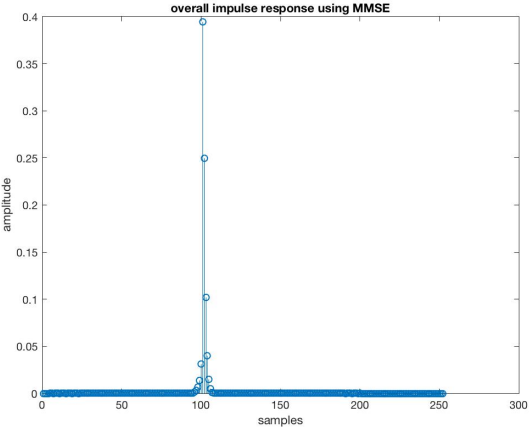


Figure 2.12: Time domain plot of MMSE-LE(N=50, SNR=1)

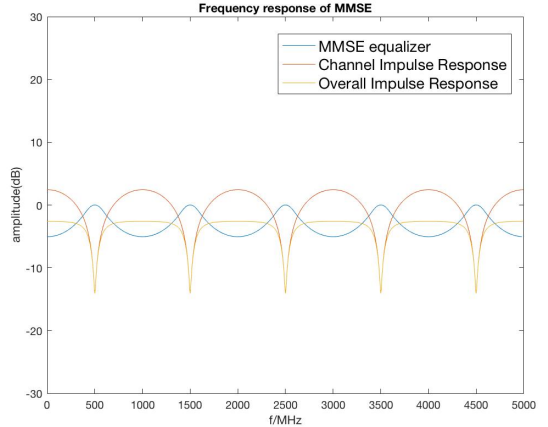


Figure 2.13: Frequency domain plot of MMSE-LE(N=50, SNR=1)

However, when the SNR is low, the high noise power does affect the resulting OCTF. In frequency domain, in order to filter noise power out, the frequency response of MMSE-LE is kept low even the frequency response of CTR meets its minimum value. As a result, the OCTF plot is worse than that in high SNR case. Due to the distorted OCTF, in time domain, the

peak in OCTF now drops to 0.4, which is far from 1. Due to this phenomenon, MMSE-LE is said to be biased equalizer.

The bias property of MMSE-LE can also be seen in Figure 2.14. Yellow plots are the symbols after ZFE and black plots are the symbols after MMSE-LE. It can be easily seen that ZFE is unbiased equalizer while MMSE-LE is biased equalizer because of the concentration of received symbols to the original point. Actually, this biased phenomenon has little effect on MPSK modulations because their decision boundaries depend on angles. However, for higher constellation such as 16QAM or 256QAM, the bias does influence the results.

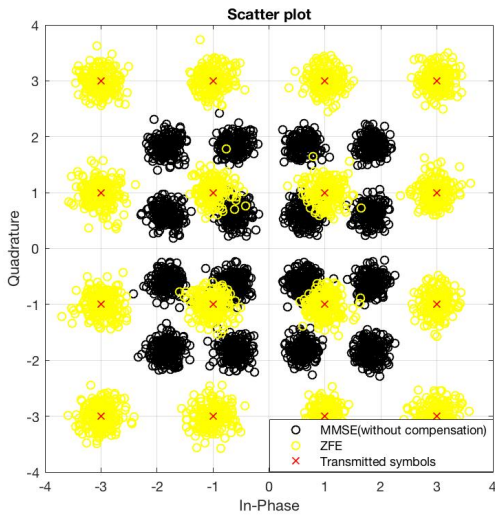


Figure 2.14: Time domain plot( $N=50$ )

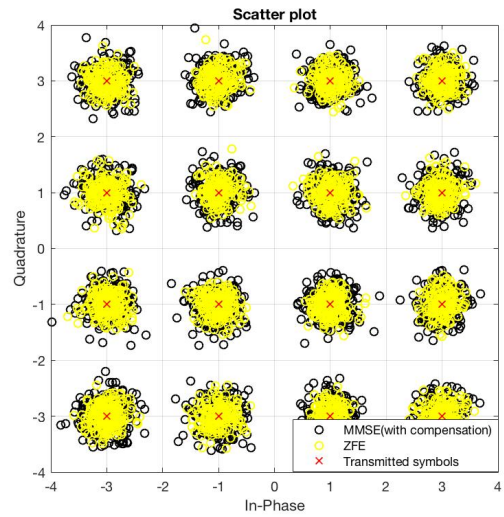


Figure 2.15: Frequency domain plot( $N=50$ )

One good way to compensate the bias phenomenon is to map the biased symbols back to its correct constellation, which can be achieved with an amplifier. The constellation after compensation is shown in Figure 2.15 which now looks correct. Moreover, the SNR of output signal( $y[k]$ ) doesn't change. That means the noise suppression property of MMSE-LE remains the same.

## 2.4 Channel Modeling

The term channel refers to the medium between the transmitting antenna and the receiving antenna. In this project, channel is characterized by  $CIR(h[k])$ . Each non-zero  $h[k]$  denotes one

path of the transmitted signal. Therefore, the task in this section is to find out what  $h[k]$  is, or which distribution  $h[k]$  follows.

To get convincing results, it is very important to build a reasonable channel model. More precise the channel is, more credible our simulations will be. However, a precise channel model might be too complicated so that it is nearly impossible to analyze the results theoretically. In addition, simulating this channel will be quite costly in time. Therefore, we first build up a simple channel model for analysis and simulation. Then, a more precise channel model from 802.15.4a is built for verification.

#### 2.4.1 Simple channel Model

The simple model introduced here is widely used in many relevant researches [1, 2, 4]. In our simple channel, each coefficient of CIR is assumed to be a circular symmetric complex Gaussian (CSCG) random variable with zero mean and

$$E[|h[k]|^2] = e^{-\frac{kT_s}{\sigma_T}}$$

where  $T_s$  is the system time resolution and  $\sigma_T$  is the root mean square of channel delay spread of the channel. It can be seen that the energy of path gain decreases exponentially. So we also call it 'exponential channel'.

Since  $c[k]$  is a CSCG random variable, its real part and imagine part follow the same Gaussian Distribution. Therefore,  $|c[k]|$ , which can be expressed as  $\sqrt{a^2[k] + b^2[k]}$ , follows Rayleigh Distribution. Then, we have

$$c[k] = a[k] + ib[k]$$

$$\text{where } a, b \sim N(0, \frac{1}{2}e^{-\frac{kT_s}{\sigma_T}})$$

The resulting power delay profile and CIR is shown in Figure 2.16 and 2.17.

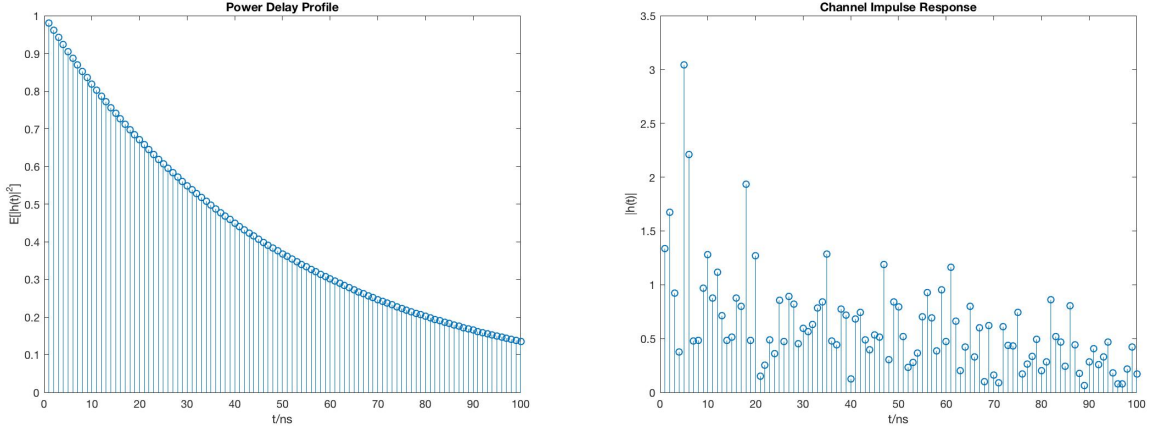


Figure 2.16: PDP of simple channel model( $T_s = 1\text{ns}$ ,  $\sigma_T = 50\text{ns}$ )

Figure 2.17: CIR of simple channel model( $T_s = 1\text{ns}$ ,  $\sigma_T = 50\text{ns}$ )

#### 2.4.2 802.15.4a Indoor Channel Model

As for the more accurate channel model, we adopt the 802.15.4a standard channel model, which is given in [20]. The CIRs are expressed using a Saleh-Valenzuela(SV) model [21], which is shown below:

$$h_{discr}(t) = \sum_{l=0}^L \sum_{k=0}^K a_{k,l} \exp(j, \phi_{k,l}) \delta(t - T_l - \tau_{k,l})$$

where  $a_{k,l}$  is the tap weight of the  $k$ th component in the  $l$ th cluster,  $T_l$  is the delay of the  $l$ th cluster,  $\tau_{k,l}$  is the delay of the  $k$ th relative delay to the  $l$ th cluster arrival time  $T_l$ . The phases  $\phi_{k,l}$  are uniformly distributed. The phase is taken as a uniformly distributed random variable from the range  $[0, 2\pi]$

For all the coefficients above, the number of clusters  $L$  follows Poisson Distribution and the distribution of  $T_l$ ,  $\tau_{k,l}$  are given by Poisson Process. Since the generation of 802.15.4a channels is quite complex, we briefly summarized the generation into two steps:

- 1) Generate the power delay profile for Saleh-Valenzuela(SV) model.
- 2) Achieve the amplitude of CIR as Nakagami-distributed variable with mean-square given by the mean power as computed before. Then compute phase for each component as uniformly distributed.

**Step 1** The power delay profile is exponential within each cluster

$$E|a_{k,l}|^2 = \Omega_l \frac{1}{\gamma_l[(1-\beta)\lambda_1 + \beta\lambda_2 + 1]} \exp(\tau_{k,l}/\gamma_l)$$

where  $\Omega_l$  is the integrated energy of the  $l$ th cluster, and  $\gamma_l$  is the intra-cluster decay time constant.  $\beta$  is the mixture probability, while  $\lambda_1$  and  $\lambda_2$  are the ray arrival rates.

The mean (over the cluster shadowing) mean (over the small-scale fading) energy of the  $l$ th cluster follows in general an exponential decay

$$10\log(\Omega_l) = 10\log(\exp(-T_l/\Gamma_l)) + M_{cluster}$$

where  $M_{cluster}$  is a normally distributed variable with standard deviation  $\sigma_{cluster}$  around it.  $\Gamma$  is the inter-cluster delay constant.

**Step 2** The distribution of small-scale amplitude is expressed as:

$$pdf(x) = \frac{2}{\Gamma(m)} \left(\frac{m}{\Omega}\right)^m x^{2m-1} \exp\left(-\frac{m}{\Omega}x^2\right),$$

where  $m \geq 0.5$  is the Nakagami m-factor,  $\Gamma(m)$  is the gamma function, and  $\Omega$  is the mean-square value of the amplitude.

The parameter  $\Omega$  corresponds to the mean power, and its delay dependence is thus given by the power delay profile above. The  $m$  parameter is modeled as a lognormally distributed random variable, whose logarithm has a mean  $\mu_m$  and standard deviation  $\sigma_m$ . Both of these are dependent on the delay, which can be expressed as  $\mu_m(\tau) = m_0 - k_m\tau$  and  $\sigma_m(\tau) = \widehat{m}_0 - \widehat{k}_m\tau$

As for the phase component, since it follows uniform distribution, it can be expresses as:

$$pdf(\phi) = \frac{1}{2\pi}, \quad \phi \in [0, 2\pi]$$

## Simulation Results

In document [20], solutions of five different environments are provided: Residential environments, Indoor office environment, Outdoor environment, Open outdoor environments and Industrial environments, where the only difference is the value of parameters. In this project, we only adopted the 802.15.4a channels for Residential environment. The CIR of LOS residential and NLOS residential environments are shown in Figure 2.18 and 2.19.

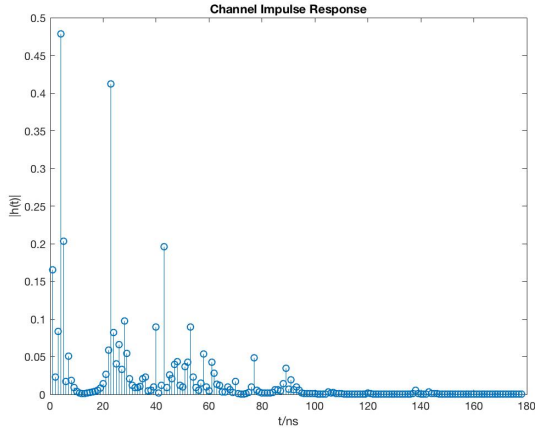


Figure 2.18: 802.15.4a LOS residential channel ( $B = 2GHz$ ,  $f_c = 6GHz$ )

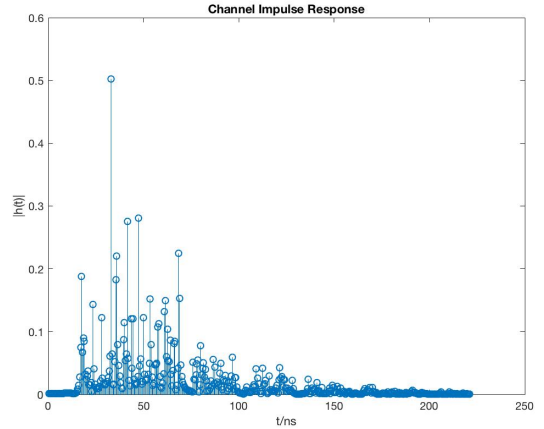


Figure 2.19: 802.15.4a NLOS residential channel ( $B = 2GHz$ ,  $f_c = 6GHz$ )

Table 2.1: Parameters for 802.15.4a residential LOS and NLOS channels [20]

Parameters	Description	LOS	NLOS
$\bar{L}$	mean value of $L$	3	3.5
$\Lambda[1/ns]$	cluster arrival rate	0.047	0.12
$\lambda_1, \lambda_2[1/ns]$	ray arrival rates	1.54,0.15,0.095	1.77,0.15,0.045
$\beta$	mixture probability	0.095	0.045
$\Gamma[ns]$	inter-cluster decay constant	22.61	26.27
$k_\gamma, \gamma_0[ns]$	intra-cluster decay parameters	0, 12.53	0, 17.50
$\sigma_{cluster}[dB]$	cluster shadowing variance	2.75	2.93
$m_0[dB], k_0$	Nakagami m factor mean	0.67,0	0.69,0
$\widehat{m}_0[dB], \widehat{k}_m$	Nakagami m factor variance	0.28,0	0.32,0

Their parameters are shown in table 2.1. In the following chapters, the 802.15.4a channel models are mainly used to verify the results got from the simple channel.

# Chapter 3

## TR Single & Multiple User Model

### 3.1 Overview

Thanks to the work in chapter 2, we can now build up TR channel models for simulation and analysis. Our work in this chapter begins with the TR single channel model and then moves on to the TR multiple user channel model, which is also called TRDMA scheme. Since we have assumed the CIRs to be perfectly known, the channel probing phase is meaningless in our simulation. Thus, we ignore the channel probing phase and only simulate the TR transmission phase. In single user case, downlink and uplink transmission are quite similar. So only downlink data transmission is analyzed. However, in multiple user case, both the downlink and uplink data transmission are analyzed due to their asymmetry.

### 3.2 TR Single User Model

The TR single user model for downlink is shown in Figure 3.1.

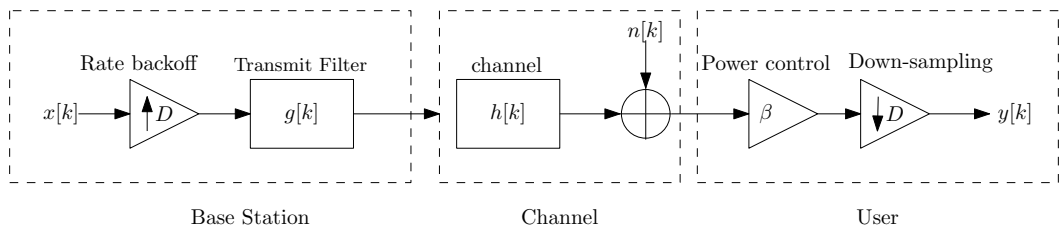


Figure 3.1: TR single user model

Here,  $g[k]$  is the normalized TR waveform, which is defined as

$$g[k] = \frac{h^*[-k]}{\sum |h[k]|^2}$$

In addition, according to the definition of TR, no receive filter and equalizer is included in the model. The rate back-off factor  $D$  is used to control the transmit speed. For instance, the highest speed is achieved when  $D = 1$ . Otherwise, there will always be  $D - 1$  zeros plugged in between each two transmitted symbols, increasing the symbol period.  $\beta$  is the power control factor, mapping the received signal to the right constellation. However, it doesn't change the value of received SNR.

Since there is no receive filter, the CTR  $h_{ct}[k]$  now can be expressed as  $h_{ct}[k] = g[k] * h[k]$ . Then, the received signal can be expressed as

$$y[k] = \underbrace{\beta x[k]h_{ct}[0]}_{Signal} + \underbrace{\beta \sum_{\substack{l=-L_D \\ l \neq 0}}^{L_D} x[k-l]h_{ct}[lD]}_{ISI} + \underbrace{\beta n[Dk]}_{Noise}$$

where  $L_D = \lfloor \frac{L}{D} \rfloor$  and  $L$  is the length of CIR. Since there is only one user, no IUI exists in this model. Then, the SINR at receiver can be calculated as shown below:

$$SINR = \frac{P_s}{P_s \sum_{\substack{l=-L_D \\ l \neq 0}}^{L_D} |h_{ct}[lD]|^2 + P_N}$$

where  $P_s$  is the symbol energy,  $P_N$  is the noise power. It is clear that the value of  $\beta$  doesn't affect the received SINR. Then, our results are shown in Figure 3.2 to Figure 3.5. In our simulation, we assume perfect synchronization between the transmitter and receiver. Besides, the system bandwidth  $B$  is set to be 1GHz, which means the time resolution is 1ns.

The impact of rate back-off factor  $D$  to the effective SINR is shown in Figure 3.2 and 3.3. Simulation results of both exponential and 802.15.4a Indoor NLOS channel show that a larger  $D$

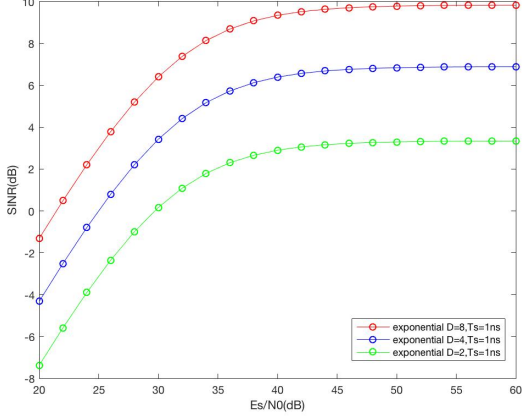


Figure 3.2: The impact of rate back-off factor D for exponential channel( $B = 1\text{GHz}$ ,  $\sigma_T = 50\text{ns}$ )

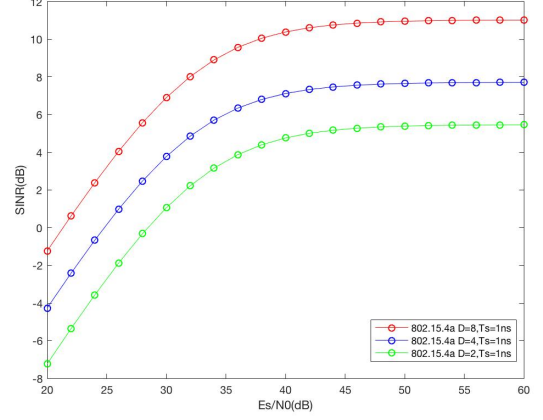


Figure 3.3: The impact of rate back-off factor D for 802.15.4a NLOS Residential channel( $B = 1\text{GHz}$ ,  $f_c = 6\text{GHz}$ )

can reduce ISI while maintaining the signal power. This result is reasonable because the increase of symbol period will separate each symbol further, decreasing the interference between each other. In the high  $E_s/N_0$  region where interference power dominates the noise power, the SINR tends to be stable and approximately a 3dB gain can be seen when the rate back-off factor D is doubled.

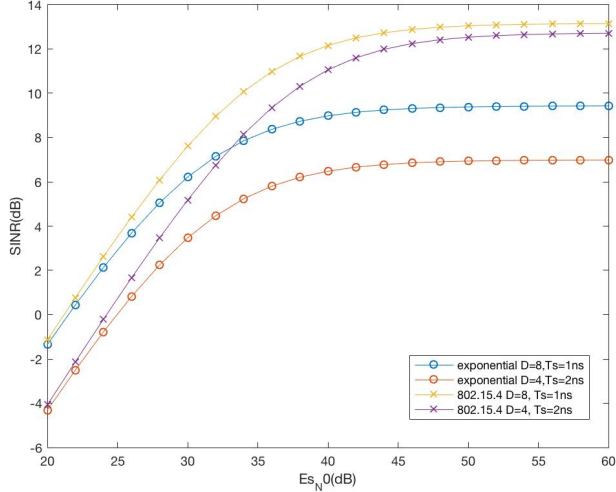


Figure 3.4: The impact of multi-path richness over SINR

Figure 3.4 shows the impact of multi-path richness to the effective SINR. Note that in Figure 3.4, we set  $D$  to 4 and 8 for the channels with  $T_s = 2\text{ns}$  and  $T_s = 1\text{ns}$ , respectively, to ensure that their baud rates(i.e. B/D) are the same for a fair comparison. As seen from this comparison, a channels multi-path richness (or higher resolution of perceiving multiple paths)

due to the broader system bandwidth, gives rise to better performance, which in essence increases the degree of freedom of the location-specific signatures. The performance improvement of exponential channel is obvious and larger than that of 802.15.4a channel model.

### 3.3 TR Multiple User Model

#### 3.3.1 Downlink For Multiple User Case

The model for downlink TR multi-user transmission is shown in Figure 3.5.

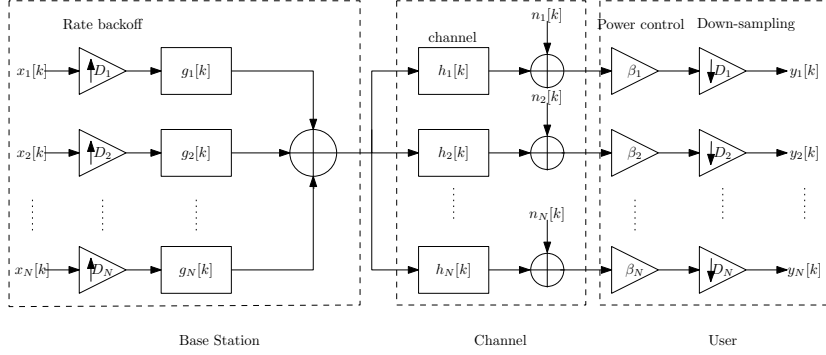


Figure 3.5: Downlink for TR multiple user model

In this transmission stage, the base station combines all the signals for different users and sends them out in one antenna. The same transmitted signal passes through different channel and reaches each user. Due to the spacial focusing property of TR, only the energy of wanted signal is concentrated for each user. In theory, each user may have different transmit speed(rate back-off factor  $D$ ) and symbol energy( $P_s$ ). However, for the convenience of simulation, we assume the factor  $D$  and  $P_s$  are the same for all users. The TR waveform  $g_j[k]$  for user  $j$  can be written as:

$$g_j[k] = \frac{h_j^*[k]}{\sum |h_j[k]|^2}$$

Suppose there are totally  $N$  users. There will be  $N$  different channels and  $N \times N$  CTRs. We have  $h_{ct}^{ij}[k] = g_i[k] * h_j[k]$ . Then, the received signal for the  $j$ th user can be expressed as:

$$\begin{aligned}
y_j[k] &= \beta_j \sum_{i=1}^N x_i[k] * h_j[k] * g_i[k] + \beta_j n[k] \\
&= \beta_j \sum_{i=1}^N x_i[k] * h_{ct}^{ij}[k] + \beta_j n[k]
\end{aligned}$$

Sampling at every  $D$  time units, we have

$$y_j[k] = \underbrace{\beta_j x_j[k] h_{ct}^{jj}[0]}_{Signal} + \underbrace{\beta_j \sum_{\substack{l=-L_D^j \\ l \neq 0}}^{L_D^j} x_j[k-l] h_{ct}^{jj}[lD]}_{ISI} + \underbrace{\beta_j \sum_{\substack{i=1 \\ i \neq j}}^N \sum_{l=-L_D^j}^{L_D^i} x_i[k-l] h_{ct}^{ij}[lD]}_{IUI} + \underbrace{\beta_j n[Dk]}_{Noise}$$

where  $L_D^j = \lfloor \frac{L^j}{D} \rfloor$  and  $L^j$  is the length for  $j$ th CIR. Now, since the IUI exists, the SINR for user  $j$  can be calculated as shown below:

$$SINR_j = \frac{P_s}{P_s \sum_{\substack{l=-L_D^j \\ l \neq 0}}^{L_D^j} |h_{ct}^{jj}[lD]|^2 + P_s \sum_{i=1}^N \sum_{l=-L_D^j}^{L_D^i} |h_{ct}^{ij}[lD]|^2 + \sigma^2}$$

Since there are multiple users, we evaluate the TR multiple user system in terms of average achievable sum rate. The achievable sum rate can be used as an important metric of the efficiency of a wireless downlink scheme, which measures the total amount of information that can be effectively delivered. Since the channel situation changes with time, we decide to use average achievable sum rate to measure the long-term performance, which is also used in [17].

$$R_{avg} = E \left[ \frac{1}{D} \sum_{j=1}^N \log_2 (1 + SINR_j) \right]$$

The performance analysis of TR multiple user downlink model is shown in Figure 3.6 and 3.7. The exponential channel and 802.15.4a channel presents the same conclusion, just like single user case.

From Figure 3.6, a larger  $D$  improves the reception quality of each symbol due to the lower

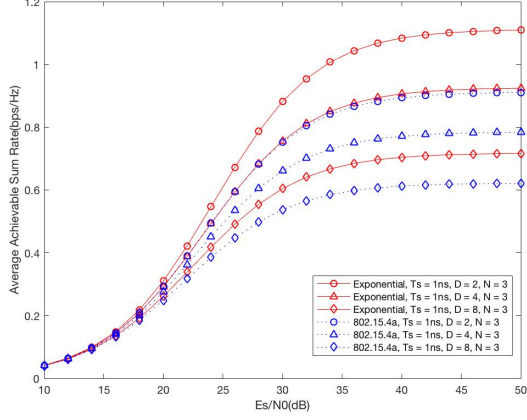


Figure 3.6: The impact of rate back-off factor  $D$  over Average Achievable Sum Rate

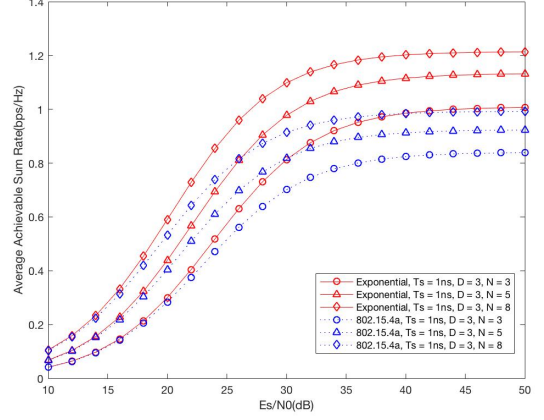


Figure 3.7: The impact of user number  $N$  over Average Achievable Sum Rate

ISI. However, it reduces the symbol rate of the transmitter. As a result, the improvement of SINR cannot compensate the loss of low symbol rates. From Figure 3.7, A larger  $N$  increases the concurrent data streams. However the stronger interference degrades the reception quality and further limit the improvement of individual achievable rate. The SINR degradation lies in the logarithm function provided before, but the increase of data streams still yield a higher sum rate when  $N$  is larger.

As a result, the choice of  $D$  and  $N$  yields an engineering tradeoff between the signal quality at each user and the sum rate of this network.

### 3.3.2 Uplink For Multiple User Case

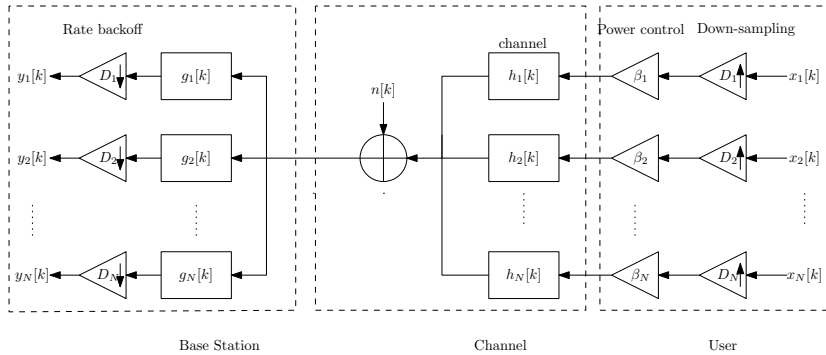


Figure 3.8: Uplink for TR multiple user model

Our focus now moves to the uplink model for TR multiple user case, which is shown in Figure 3.8.  $N$  users simultaneously transmit independent messages( $x_1[k], x_2[k], \dots, x_N[k]$ ) to the base

station through multi-path channel. Similar to downlink transmission, each user has the same D factor and the same symbol energy  $P_s$ . It can be seen that the components in base station side and user side remain the same as downlink transmission, which keeps the complexity in user side to the lowest level. The only difference is the direction of data transmission.

However, due to the asymmetry of downlink and uplink model, whether uplink data transmission enjoys the temporal focusing and spacial focusing remains unknown. As a result, the main task in this section is to explore the feasibility of this TR uplink model.

From Figure 3.8, the signal at BS can be expressed as:

$$r[k] = \sum_{i=1}^N \beta_i x_i[k] * h_i[k] + n[k]$$

Then, the received signal of BS for user  $j$  is the convolution of  $r[k]$  and  $g_j[k]$ , which is

$$\begin{aligned} y_j[k] &= \sum_{i=1}^N \beta_i x_i[k] * h_i[k] * g_j[k] + n[k] * g_j[k] \\ &= \sum_{i=1}^N \beta_i x_i[k] * h_{ct}^{ji}[k] + \tilde{n}[k] \end{aligned}$$

where  $\tilde{n}[k]$  is colored Gaussian noise. Here, we can see that the received signal for user  $j$  is almost the same as that in downlink transmission except for the noise and power control factor( $\beta$ ). Sampling  $y_j[k]$  every  $D_j$  time units, we have

$$y_j[k] = \underbrace{\beta_j x_j[k] h_{ct}^{jj}[0]}_{\text{Signal}} + \beta_j \underbrace{\sum_{\substack{l=-L_D^j \\ l \neq 0}}^{L_D^j} x_j[k-l] h_{ct}^{jj}[lD]}_{\text{ISI}} + \underbrace{\sum_{\substack{i=1 \\ i \neq j}}^M \beta_i \sum_{l=-L_D^j}^{L_D^i} x_i[k-l] h_{ct}^{ji}[lD]}_{\text{IUI}} + \underbrace{\tilde{n}[Dk]}_{\text{Noise}}$$

Examining the results of downlink and uplink, the same mathematical structure can be found. As a result, the temporal focusing and spacial focusing effect observed in downlink transmission can also be achieved in TR uplink scheme. Unlike the physical spacial focusing effect in the downlink where the useful signal energy is concentrated at different physical locations, in uplink scenario, the signal power is focused in the users' signature waveform space.

Such a virtual spacial focusing effect enables the Base station to use the users' specific signature waveform to get the wanted signal out of the combined received signal from different users, allowing them to access BS at the same time.

The SINR for user  $j$  can be expressed as:

$$SINR_j = \frac{\beta_j^2 P_s}{\beta_j^2 P_s \sum_{\substack{l=-L_D^j \\ l \neq 0}}^{L_D^j} |h_{ct}^{jj}[lD]|^2 + P_s \sum_{i=1}^N \beta_i^2 \sum_{l=-L_D^j}^{L_D^i} |h_{ct}^{ji}[lD]|^2 + \widetilde{\sigma^2}}$$

From the previous discussion, we can see that the asymmetry of downlink and uplink transmission does not bring much difference in SINR. Since there is trivial difference between TR downlink and uplink transmission, the performance of uplink should be similar with that of downlink. It is unnecessary to analyze the same performance again. Also, in the next chapter about waveform design, only downlink transmission is considered in multiple user case.

# Chapter 4

## Waveform Design

### 4.1 Overview

In chapter 3, we have analyzed the performance of TR models and explored the relationship between SINR,  $N$  and  $D$ . With the increase of  $N$ , the signal quality will get worse while the number of data streams increases. With the increase of  $D$ , the transmitted signal will have better quality, but the transmit speed will get lower.

In some applications such as video streams, high data rate is critical. To increase the data rate, we need to decrease  $D$  to enlarge the transmit speed. Also, as a multiple access scheme, the TR system should handle as many users as possible. However, as mentioned before, with the decrease of  $D$  and increase of  $N$ , there will be severe data quality issues due to the ISI and IUI that limit our system performance.

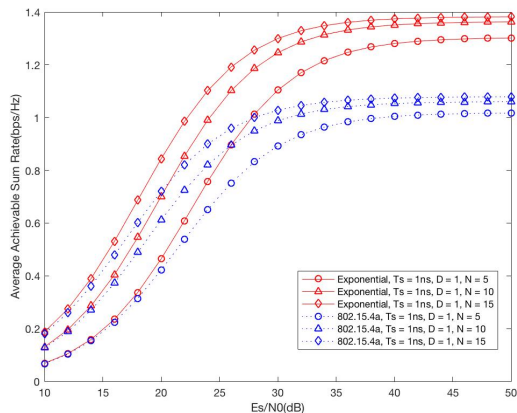


Figure 4.1: Average Achievable Sum Rate under high data transmit speed

This performance degradation can be further illustrated by Figure 4.1, where  $D = 1$  and  $N$  increases from 5 to 15. It is obvious that the achievable sum rate doesn't get much improvement even the number of users grows from 5 to 15. That means the individual achievable rates for each user has been greatly eroded by the severe ISI and IUI presented in TR system.

Next, our work is to modify existing TR models to improve the system performance in high transmit speed and high user density scenarios. Our first attempt is to introduce the idea of equalization into TR system. Then, we try to calculate the optimal waveform to get the minimum MSE. However, using the latter method, the performance improvement comes with a dramatic increase of complexity.

## 4.2 Combination of TR system and Equalizers

In this section, equalizers are provided to TR single user model first. The resulting model is presented in Figure 4.2.

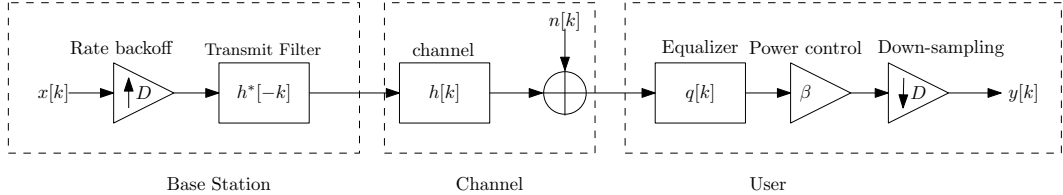


Figure 4.2: TR single user model with equalizers

Note that equalizers are placed in the user side. By doing this, the complexity of user devices is increased, which is not expected. As a result, we decide to move the equalizer to the BS size and thus remain the user complexity to the lowest level. This idea is called pre-equalization, which is firstly discussed in [22]. The modified system is shown in Figure 4.3.

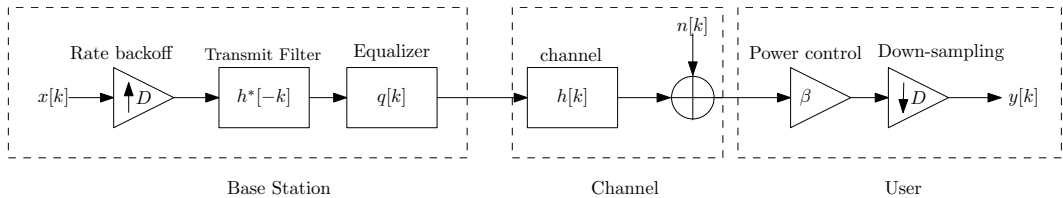


Figure 4.3: TR single user model with pre-equalization

In Figure 4.3, the equalizer is moved to the BS side. The difference between pre-equalization

and normal equalization is that, noise does not pass the equalizer in pre-equalization. As a result, the noise problem in ZFE doesn't exist anymore. Furthermore, the calculation of MMSE-LE should be somehow modified to get rid of the noise power. The only modification will be  $\phi_{dd}[\lambda] = h_{ct}[\lambda] * h_{ct}^*[-\lambda]$  and  $\varphi_{dx}[\lambda] = h_{ct}[\lambda]$ .

The performances of raw TR waveform, ZFE pre-equalization and MMSE-LE pre-equalization are measured with their Symbol Error Rates(SER), as shown in Figure 4.4 and 4.5. During this simulation, the coefficients of both ZFE and MMSE-LE have a length of 51. Additionally, the exponential channel in Chapter 2 is used with  $\sigma_T = 50ns$  and  $T_s = 1ns$ . It is clear that the SERs get improved for both  $D = 1$  and  $D = 3$  case. In addition, pre-equalization with MMSE-LE is better than ZFE in both case.

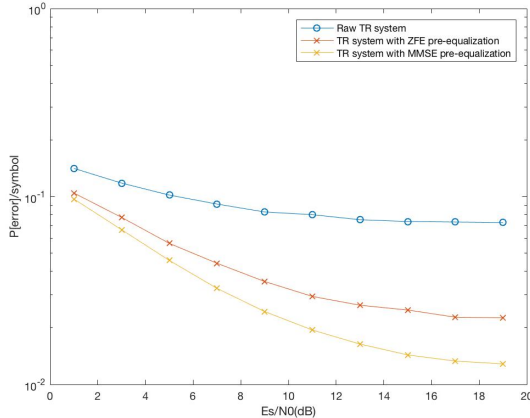


Figure 4.4: Symbol Error Rate when  $D = 1$ (BPSK, exponential channel)

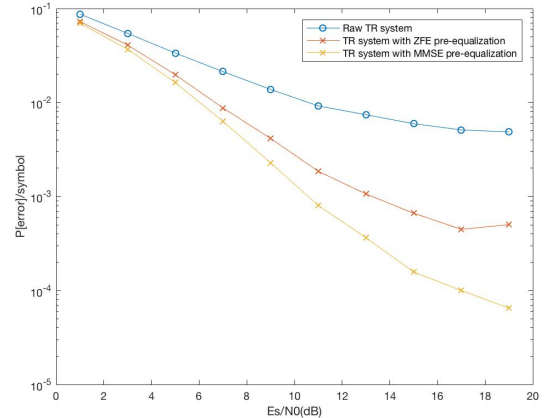


Figure 4.5: Symbol Error Rate when  $D = 3$ (BPSK, exponential channel)

However, although system performance gets improved with pre-equalization, the symbol error rate is still not acceptable, especially when  $D$  equals to 1. As a result, we then get rid of the idea of equalization and try to find the optimal wave with the least mean square error. However, with the optimal waveform, the system is not seriously a TR system. This is discussed in the following sections.

## 4.3 Optimal Waveform Design

### 4.3.1 Idea of Waveform Optimization

The idea of waveform optimization is clearly demonstrated in Figure 4.6.

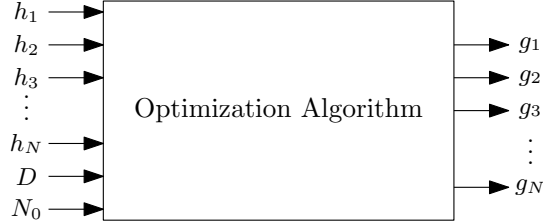


Figure 4.6: Idea of waveform optimization

Suppose there are  $N$  users in total. Their unique CIRs towards BS are  $\mathbf{h}_1, \mathbf{h}_2, \dots, \mathbf{h}_N$  and their transmit waveforms are  $\mathbf{g}_1, \mathbf{g}_2, \dots, \mathbf{g}_N$ . The optimization algorithm takes the CIRs, rate back-off factor and the noise power as inputs and the output is the waveforms with the minimum mean square error(MSE). To find out the optimization algorithm, our first job is to express our TR models in vector forms, which is discussed in the next subsection.

### 4.3.2 Vector Expression of TR System

#### TR Single User Case

The received signal is already given in section 3.2. We denote  $h[k]$  by a vector  $\mathbf{h}$  of size  $L$ . Its Toeplitz matrix of size  $(2L - 1) \times L$  is expressed as  $\mathbf{H}$ , with the first row being  $[h[0], 0_{1 \times 2L}]$  and first column being  $[h, 0_{1 \times (L-1)}]^T$ . Then the received signal can be expressed as

$$y[k] = \beta x[k] \mathbf{h}_{L\mathbf{g}} + \beta \sum_{\substack{l=-L_D \\ l \neq 0}}^{L_D} x[k+l] \mathbf{h}_{L+lD\mathbf{g}} + \beta \mathbf{n}$$

where  $\mathbf{h}_k$  is the  $k$ th row of  $\mathbf{H}$  and  $\mathbf{n}$  is the noise vector.

#### TR Multiple User Case

The received signal at user  $j$  is discussed in section 3.3. The same logic of TR single user model can be applied here. The CIR of multiple channel between BS and user  $j$  is denoted by  $\mathbf{h}_j$  with

a length of  $L_j$  and its Toeplitz matrix is expressed as  $\mathbf{H}_j$ . Then we have

$$y_j[k] = \beta_j x_j[k] \mathbf{h}_j^{L_j} \mathbf{g}_j + \beta_j \sum_{\substack{l=-L_D \\ l \neq 0}}^{L_D} x_j[k-l] \mathbf{h}_j^{L_j+lD} \mathbf{g}_j + \beta_j \sum_{\substack{i=1 \\ i \neq j}}^N \sum_{l=-L_D}^{L_D} x_i[k-l] \mathbf{h}_j^{L_j+lD} \mathbf{g}_i + \beta_j \mathbf{n}_i$$

where  $\mathbf{h}_i^k$  is the  $k$ th row of matrix  $H_i$ ,  $\mathbf{g}_i$  is the transmit waveform for user  $i$ . The derivation of these equations is included in Appendix.

#### 4.3.3 Optimal Waveform For Single User Case

The optimal waveform appears only when the MSE gets its minimum value. The MSE in single user model can be expressed as:

$$\begin{aligned} MSE(g, \beta) &= E[|e[k]|^2] \\ &= E[|y[k] - x[k]|^2] \\ &= P_s |\beta \mathbf{h}_L \mathbf{g} - 1|^2 + P_s \beta^2 \sum_{\substack{l=-L_D \\ l \neq 0}}^{L_D} |\mathbf{h}_{L+lD} \mathbf{g}|^2 + \beta^2 P_N \\ &= \beta^2 P_s \mathbf{g}^H \left( \sum_{l=-L_D}^{L_D} \mathbf{h}_{L+ld} \mathbf{h}_{L+ld}^H \right) \mathbf{g} - \beta P_s \mathbf{h}_L \mathbf{g} - \beta P_s \mathbf{g}^H \mathbf{h}_L^H + P_s + \beta^2 P_N \end{aligned}$$

where  $P_s$  is the symbol power and  $P_N = \sigma_N^2$  is the noise power. Then, to simplify our computation, we suppose  $\mathbf{h}_L \mathbf{g}$  is equal to 1 so that the received signal is already on the correct constellation. As a result,  $\beta$  can just be set to 1. The process of getting the optimal waveform  $\mathbf{g}$  can then be interpreted as an optimization problem:

$$\begin{aligned} \text{Minimize } & \mathbf{g}^H \left( \sum_{l=-L_D}^{L_D} \mathbf{h}_{L+ld}^H \mathbf{h}_{L+ld} \right) \mathbf{g} - \mathbf{h}_L \mathbf{g} - \mathbf{g}^H \mathbf{h}_L^H + 1 + \frac{P_N}{P_s} \\ \text{subject to } & \mathbf{h}_L \mathbf{g} = 1 \end{aligned}$$

Luckily, this is a convex optimization problem and the optimal waveform follows the KarushKuhnTucker(KKT) optimality conditions. The KKT condition can be written as

$$\begin{cases} \frac{\partial MSE(g)}{\partial g} + \lambda \mathbf{h}_L = 0 \\ \mathbf{h}_L \mathbf{g} = 1 \end{cases}$$

After solving the above equations, we can get the resulting optimal waveform as shown below.

The derivation is left in Appendix B.

$$\mathbf{g}_{omp} = \frac{\mathbf{h}_L \widehat{\mathbf{H}}^{-1}}{\mathbf{h}_L \widehat{\mathbf{H}}^{-1} \mathbf{h}_L^H}$$

$$\text{where } \widehat{\mathbf{H}} = \sum_{l=-L_D}^{L_D} \mathbf{h}_{L+ld}^H \mathbf{h}_{L+ld}.$$

The resulting CTR is shown in Figure 4.8 and 4.9.

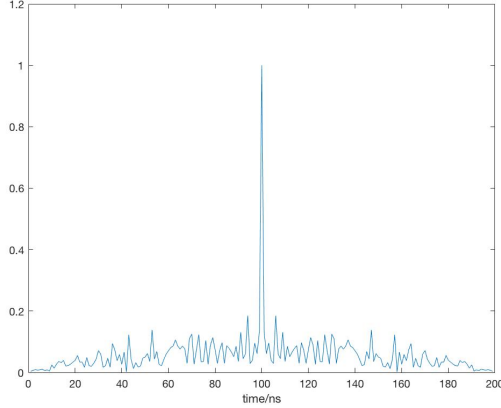


Figure 4.7: Channel Transfer Response with Raw TR waveform

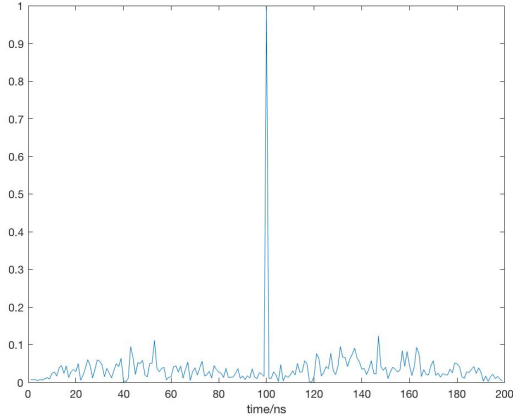


Figure 4.8: Channel Transfer Response with optimal waveform( $D = 1$ )

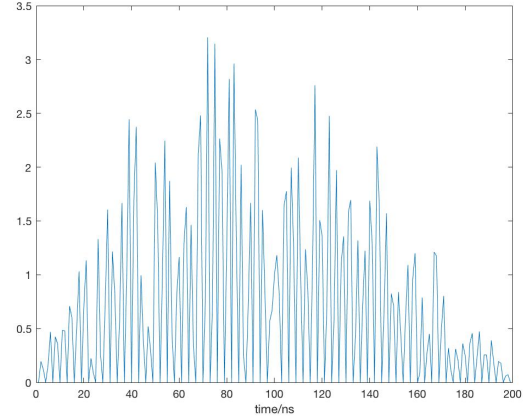


Figure 4.9: Channel Transfer Response with optimal waveform( $D = 3$ )

Compared with the raw CTR shown in Figure 4.8, it is obvious that the ISI is suppressed

when  $D$  equals to 1. In contrast, the resulting waveform for  $D = 3$  does not seem nice at the first glance. However, the ISI does drop greatly from the fact that the CTR is forced to nearly zero for every three time units except the central point. Actually, the extremely high values seen in Figure 4.9 do not influence any other symbols since the symbols are transmitted every three time units. Due to the obvious suppression of ISI, the system performance gets improved greatly and is shown in Figure 4.10 and 4.11.

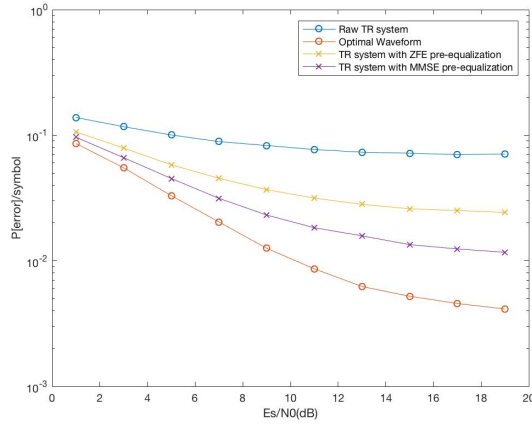


Figure 4.10: Symbol Error Rate comparison with optimal waveform( $D = 1$ )

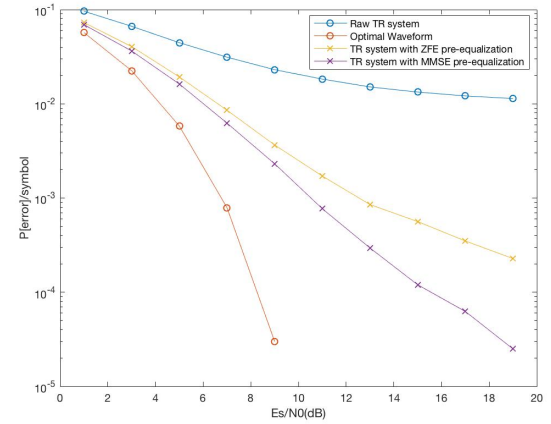


Figure 4.11: Symbol Error Rate comparison with optimal waveform( $D = 3$ )

Compared with the pre-equalization, the optimal waveform further reduces the SER, especially when  $D$  is large. Because of the progress with optimal waveform design, it is reasonable to apply the same logic to multiple user case.

#### 4.3.4 Optimal Waveforms For Multiple User Case

##### Two User Case

The optimum waveform design for two user case is considered first. For convenience, we assume that they have the same symbol energy, rate back-off factor  $D$  and CIR length. There are two unique channels  $\mathbf{h}_1$  and  $\mathbf{h}_2$  with a length of  $L$  respectively. Then, there are two waveforms,  $\mathbf{g}_1$  and  $\mathbf{g}_2$ , for each user. Same as single user case,  $\mathbf{H}_1$  and  $\mathbf{H}_2$  are introduced to represent the Toeplitz matrix of  $\mathbf{h}_1$  and  $\mathbf{h}_2$  with a size of  $(2L - 1) \times (2L - 1)$ . Then, the mean square error

for each user can be expressed as

$$MSE_1(g1, g2) = P_s |\mathbf{h}_1^L \mathbf{g}_1 - 1|^2 + P_s \sum_{\substack{l=-L_D \\ l \neq 0}}^{L_D} |\mathbf{h}_1^{L+ld} \mathbf{g}_1|^2 + P_s \sum_{l=-L_D}^{L_D} |\mathbf{h}_1^{L+ld} \mathbf{g}_2|^2 + P_N$$

$$MSE_2(g1, g2) = P_s |\mathbf{h}_2^L \mathbf{g}_2 - 1|^2 + P_s \sum_{\substack{l=-L_D \\ l \neq 0}}^{L_D} |\mathbf{h}_2^{L+ld} \mathbf{g}_2|^2 + P_s \sum_{l=-L_D}^{L_D} |\mathbf{h}_2^{L+ld} \mathbf{g}_1|^2 + P_N$$

where  $\mathbf{h}_i^k$  means the  $k$ th row of  $\mathbf{H}_i$ ,  $P_s$  is the symbol energy and  $P_N$  denotes the variance of noise.

The goal here is to minimum the overall  $MSE$ , which is  $MSE_1 + MSE_2$ . However, to solve an optimization problem with two variable vectors is quite difficult. As a result, we combine  $\mathbf{g}_1$

and  $\mathbf{g}_2$  together and create a vector  $\mathbf{g}$  where  $\mathbf{g} = \begin{bmatrix} \mathbf{g}_1 \\ \mathbf{g}_2 \end{bmatrix}$

Then the overall mean square error can be written as

$$\begin{aligned} MSE(\mathbf{g}) &= MSE_1(\mathbf{g}_1, \mathbf{g}_2) + MSE_2(\mathbf{g}_1, \mathbf{g}_2) \\ &= P_s \mathbf{g}^H \widehat{\mathbf{H}} \mathbf{g} - P_s \mathbf{h}_L \mathbf{g} - P_s \mathbf{g}^H \mathbf{h}_L^H + 2P_s + 2P_N \end{aligned}$$

where  $\widehat{\mathbf{H}} = \begin{bmatrix} \widehat{\mathbf{H}}_1 & \widehat{\mathbf{H}}_2 \\ \mathbf{0}_{L \times L} & \widehat{\mathbf{H}}_1 + \widehat{\mathbf{H}}_2 \end{bmatrix}$ ,  $\widehat{\mathbf{H}}_i = \sum_{l=-L_D}^{L_D} \mathbf{h}_i^{L+ld} \mathbf{h}_i^{L+ld}$  and  $\mathbf{h}_L = [\mathbf{h}_1^L \quad \mathbf{h}_2^L]$ . Now,

the equation is very similar with the equation in previous section and the whole problem can be transferred into an optimization problem again.

$$\text{Minimize } \mathbf{g}^H \widehat{\mathbf{H}} \mathbf{g} - \mathbf{h}_L \mathbf{g} - \mathbf{g}^H \mathbf{h}_L^H + 2 + \frac{2P_N}{P_s}$$

$$\text{subject to } \widehat{\mathbf{h}}_i \mathbf{g} = 1, \quad i = 1, 2$$

The KKT condition can then be written into

$$\left\{ \begin{array}{l} \frac{\partial MSE(g)}{\partial g} + \lambda_1 \widehat{\mathbf{h}}_1 + \lambda_2 \widehat{\mathbf{h}}_2 = 0 \\ \widehat{\mathbf{h}}_1 \mathbf{g} = 1 \\ \widehat{\mathbf{h}}_2 \mathbf{g} = 1 \end{array} \right.$$

where  $\widehat{\mathbf{h}}_1 = \begin{bmatrix} \mathbf{h}_1^L & \mathbf{0}_{1 \times L} \end{bmatrix}$  and  $\widehat{\mathbf{h}}_2 = \begin{bmatrix} \mathbf{0}_{1 \times L} & \mathbf{h}_2^L \end{bmatrix}$  Then the optimal waveform for two user case can be calculated as shown below:

$$\mathbf{g}_{omp} = [(\alpha \widehat{\mathbf{h}}_1 - \beta \widehat{\mathbf{h}}_2) \widehat{\mathbf{H}}^{-1}]^H$$

$\alpha$  and  $\beta$  can be computed by  $\begin{bmatrix} \alpha & \beta \end{bmatrix}^T = \boldsymbol{\Omega}^{-1} I$ , where  $\boldsymbol{\Omega} = \begin{bmatrix} \widehat{\mathbf{h}}_1 \widehat{\mathbf{H}}^{-1} \widehat{\mathbf{h}}_1^H & \widehat{\mathbf{h}}_1 \widehat{\mathbf{H}}^{-1} \widehat{\mathbf{h}}_2^H \\ \widehat{\mathbf{h}}_2 \widehat{\mathbf{H}}^{-1} \widehat{\mathbf{h}}_1^H & \widehat{\mathbf{h}}_2 \widehat{\mathbf{H}}^{-1} \widehat{\mathbf{h}}_2^H \end{bmatrix}$  and  $I = \begin{bmatrix} 1 & 1 \end{bmatrix}^T$  Then D is set to 1 and the resulting CTRs are shown in Figure 4.12 to 4.15.

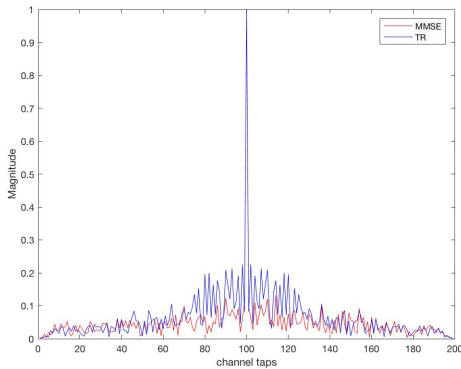


Figure 4.12: Channel Transfer Response of user 1 signal at user 1

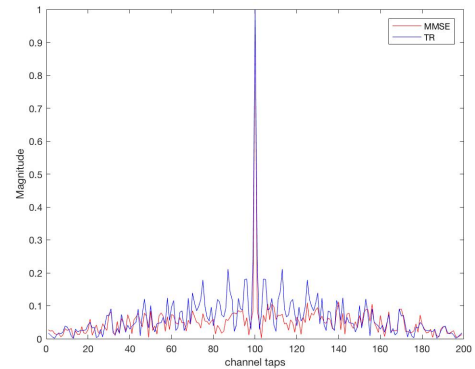


Figure 4.13: Channel Transfer Response of user 2 signal at user 2

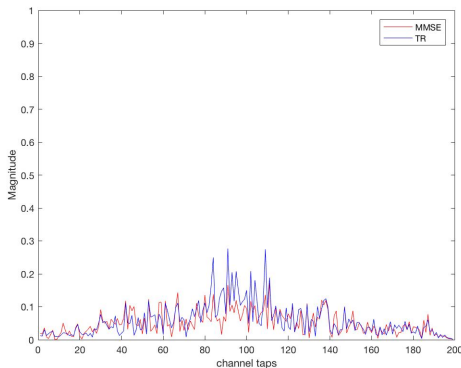


Figure 4.14: Channel Transfer Response of user 1 signal at user 2

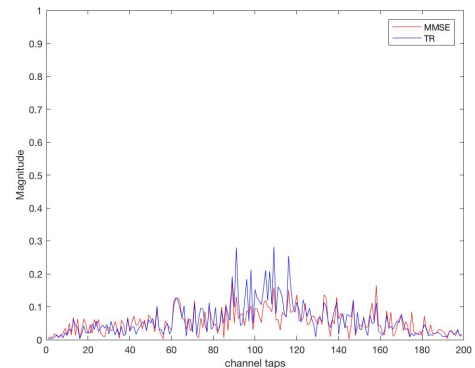


Figure 4.15: Channel Transfer Response of user 2 signal at user 1

In Figure 4.12 and 4.13, the comparison of raw TR waveform and optimal MMSE waveform shows that the user signal is better concentrated at the center after waveform optimization and thus reduces ISI. In Figure 4.14 and 4.15, the optimal MMSE waveform imposes less interference to the other users. That means TR system after waveform optimization enjoys a better spacial focusing effect which reduces IUI.

The system performance improvement is shown in Figure 4.16. As can be seen from Figure 4.16, the average achievable sum rate is largely improved compared to the raw TR multiple user model.

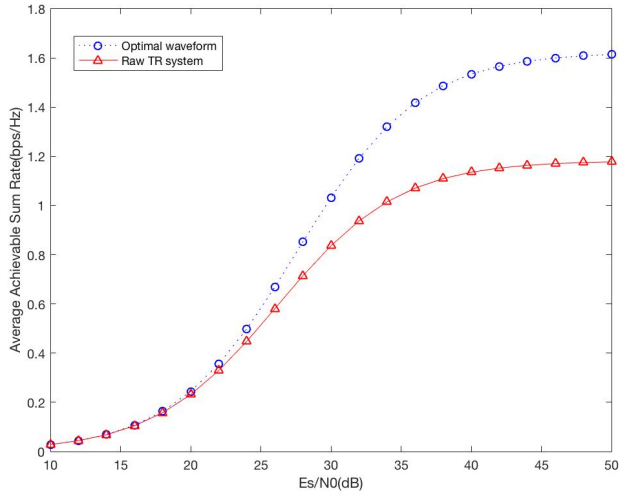


Figure 4.16: Average Achievable Sum Rate with and without waveform optimization( $D = 1$ )

### Multiple User Case

Here our goal is to apply the same logic to more than two users. Suppose there are  $N$  users, each with a unique channel  $\mathbf{h}_1, \mathbf{h}_2, \dots, \mathbf{h}_N$  with the same length  $L$ . Then, there are  $N$  waveforms,  $\mathbf{g}_1, \mathbf{g}_2, \dots, \mathbf{g}_N$ , for each user. Again,  $\mathbf{H}_1, \mathbf{H}_2, \dots, \mathbf{H}_N$  are introduced as the Toeplitz matrix for all the channel responses. Again, to get the optimal waveform, we combine all the transmit waves into one vector  $\mathbf{g}$ . Then, the total mean square error can be expressed as

$$\begin{aligned}
MSE(\mathbf{g}) &= \sum_{i=1}^N MSE_i(\mathbf{g}_1, \mathbf{g}_2, \dots, \mathbf{g}_N) \\
&= \mathbf{g}^H \widehat{\mathbf{H}} \mathbf{g} - \mathbf{h}_L \mathbf{g} - \mathbf{g}^H \mathbf{h}_L^H + N + N\sigma_N^2
\end{aligned}$$

where each component can be expressed as

$$\widehat{\mathbf{H}} = \begin{bmatrix} \sum_{i=1}^N \widehat{\mathbf{H}}_i & \mathbf{0}_{L \times L} & \cdots & \mathbf{0}_{L \times L} \\ \mathbf{0}_{L \times L} & \sum_{i=1}^N \widehat{\mathbf{H}}_i & \cdots & \mathbf{0}_{L \times L} \\ \vdots & \vdots & \ddots & \vdots \\ \mathbf{0}_{L \times L} & \mathbf{0}_{L \times L} & \cdots & \sum_{i=1}^N \widehat{\mathbf{H}}_i \end{bmatrix}, \mathbf{h}_L = \begin{bmatrix} \mathbf{h}_1^L & \mathbf{h}_2^L & \cdots & \mathbf{h}_N^L \end{bmatrix}$$

Then, the optimization problem can be written as

$$\text{Minimize } \mathbf{g}^H \widehat{\mathbf{H}} \mathbf{g} - \mathbf{h}_L \mathbf{g} - \mathbf{g}^H \mathbf{h}_L^H + N + \frac{NP_N}{P_s}$$

$$\text{subject to } \widehat{\mathbf{h}}_i \mathbf{g} = 1, \quad i = 1, 2, \dots, N$$

where  $\mathbf{h}_i^L = \begin{bmatrix} \mathbf{0}_{1 \times (i-1)L} & \mathbf{h}_i^L & \mathbf{0}_{1 \times (N-i)L} \end{bmatrix}$ . The optimal waveforms for  $N$  users can then be

calculated

$$\mathbf{g}_{omp} = \left[ \sum_{i=1}^N \lambda_i \widehat{\mathbf{h}}_i \widehat{\mathbf{H}}^{-1} \right]^H$$

$\lambda_i$  can be solved from  $\begin{bmatrix} \lambda_1 & \lambda_2 & \dots & \lambda_N \end{bmatrix}^T = \Omega^{-1} \mathbf{I}$  where  $\Omega$  is a  $N \times N$  matrix and the element on  $i$ th row and  $j$ th column is  $\widehat{\mathbf{h}}_i \widehat{\mathbf{H}}^{-1} \widehat{\mathbf{h}}_j^H$ .  $\mathbf{I}$  is a column vector of length  $N$  where each element is 1. The performance after waveform optimization is shown in Figure 4.17 to 4.19.

From the simulation results, the system performances do get improved when  $D$  is equal to 1, 3 and 5. When  $D$  gets larger, the improvement grows. For the extreme condition where  $D$  equals to 1, the system performance is not improved very much. That is because the transmit speed is so large that it is nearly impossible to eliminate all the ISI and IUI. In other words,

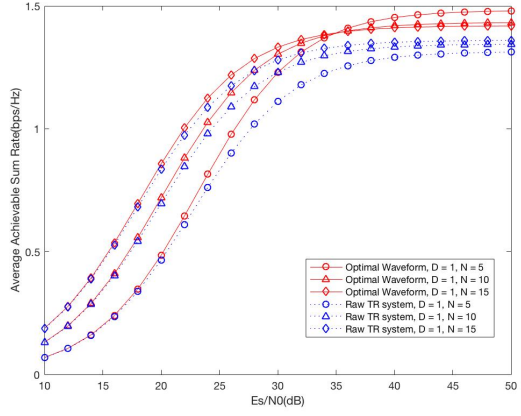


Figure 4.17: Average Achievable Sum Rate with and without waveform optimization( $D = 1$ )

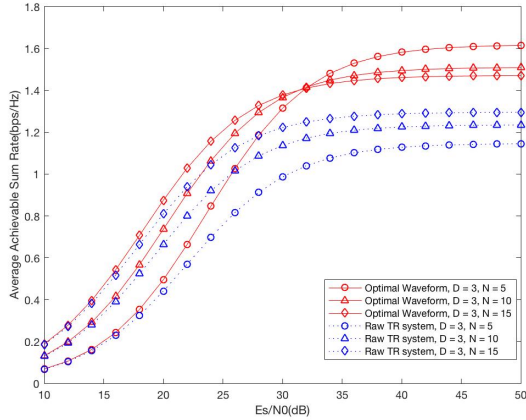


Figure 4.18: Average Achievable Sum Rate with and without waveform optimization( $D = 3$ )

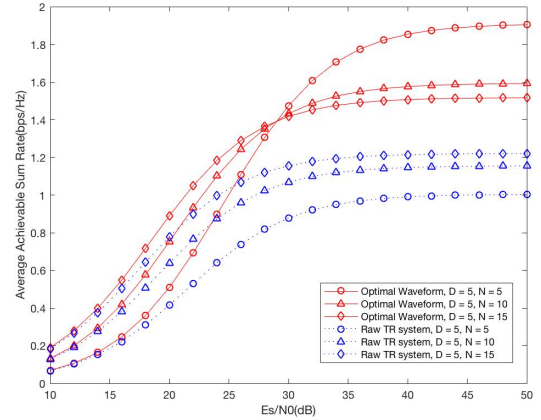


Figure 4.19: Average Achievable Sum Rate with and without waveform optimization( $D = 5$ )

when  $D$  equals to 1, every position in CTR interference with other symbols and users. However, for the lower transmit speed( $D = 3, 5$ ), there are positions in CTR that will not interfere with other symbols and users. As a result, it is possible to force the interference points small and move those energy to the non-interference points.

Also, it is obvious that for all simulation results with optimization algorithm, the system performance with less user( $N = 5$ ) gets better Achievable Sum Rate than high user density case( $N = 10, 15$ ). That means our optimization algorithm is also greatly limited by the number of users, even it is the optimal solution.

#### 4.3.5 Concerns With Waveform Optimization

Although the system performance with optimization algorithm looks good, there are still three concerns that limit its applications in the real world. The first one is transmit energy. In all simulations, we assume that  $\mathbf{h}_i^L \mathbf{g} = 1$ . It does simplify our computation. However, if the CIR is quite small, the resulting transmit waveform  $\mathbf{g}$  might be extremely large and the transmit energy is not acceptable in the reality. Therefore, it is necessary to add power control mechanism in the optimization algorithm to limit the transmit power. But this time the optimization problem will be even harder to solve.

The next concern is the computation complexity. This problem is obvious in multiple user case. For instance, if we have 10 users and the length of CIR is 100, we have to deal with  $\widehat{\mathbf{H}}$  with a size of  $1000 \times 1000$  and try to get its inverse. For a  $L \times L$  matrix, the computation complexity is  $\mathcal{O}(L^3)$ . That way, the complexity is extremely large. However, considering the special structure of  $\widehat{\mathbf{H}}$ , there are probably existing algorithms to reduce the computation complexity dramatically.

The last concern is synchronization. From Figure 4.9, it is obvious that the energy at non-interference points is quite large. If our TR system meets a synchronization problem, the interference than could be very large and ruin all the symbols totally.

### 4.4 Possible Future Work

There are a lot of works remaining in waveform design process. First, more advanced and complex equalizers can be applied in pre-equalization to improve the system performance. Besides, different combinations of linear equalizers also deserve a try. Second, add extra constraints to the optimization problem to limit the transmitted power and try to solve it. Third, find proper algorithm to solve the optimization in a easier way. Last, use the idea of interference pre-cancellation to eliminate the ISI. This is already attempted by Yu-Han Yang and K. J. Ray Liu [19].

# Chapter 5

## Conclusion

This report shows that TR transmission system is a high energy efficient and low complexity wireless communication scheme. By receiving pilot pulses from the receiver and sending back the reversed waveforms, the transmitter can focus the signal energy in both spacial and time domain with high resolution, thus reducing the interference to other users. However, in high transmit speed and large user density scenarios, the ISI and IUI in TR system is still large and limit the system performance. Thus, equalization and optimization algorithm are applied to improve the performance of TR systems. The system performance can be improved with the idea of pre-equalization. We use pre-equalization because it is able to keep the complexity of user devices at a low level. Besides, the system performance can be further enhanced with the idea of MMSE. However, the improvement comes with high computational complexity of optimal waveforms.

In this degree project, our work can be summarized as follows:

- Built up a discrete-time baseband equivalent channel model. by simulating an ideal AWGN channel, adding two kinds of linear equalizers and modeling the multi-path channel.
- Then build up one TR single user model and multiple user model and analyze their performance with different  $D$  and  $N$ .
- Finally, we improved the system performance by first adding linear equalizers and then introducing optimization algorithm to minimize the mean square error.

## Appendix A.

# Derivation of MMSE-LE FIR Coefficients

To get the MMSE-LE coefficients, our first step is to calculate the differentiation of cost function  $J(\mathbf{q})$ . The rules for differentiation of scalar functions is shown below:

$$\frac{\partial}{\partial \mathbf{q}} \mathbf{q} \Phi_{dd} \mathbf{q}^H = \Phi_{dd} \mathbf{q}^H$$

$$\frac{\partial}{\partial \mathbf{q}} \mathbf{q} \varphi_{dx} = \varphi_{dx}$$

$$\frac{\partial}{\partial \mathbf{q}} \varphi_{dx}^H \mathbf{q}^H = 0$$

Then, applying these rules, we have  $\frac{\partial J(\mathbf{q})}{\partial \mathbf{q}} = \Phi_{dd} \mathbf{q}^H - \varphi_{dx}$ . Let it to be 0, we can get the optimal  $\mathbf{q}$  which is  $(\Phi_{dd}^{-1} \varphi_{dx})^H$ , just as equation 2.4.

However, to calculate the FIR coefficients, another step is to get the expression of the autocorrelation function  $\phi_{dd}[\lambda]$  of  $d[k]$  and cross-correlation function  $\varphi_{dx}[\lambda]$  between  $d[k]$  and  $x[k - k_0]$ . Note that  $d[k] = x[k] * h_{ct}[k] + n[k] = \sum_{m=-\infty}^{+\infty} x[m]h[k-m] + n[k]$ .

Another thing we need to know is the autocorrelation function  $\phi_{xx}[\lambda]$  of  $x[k]$ , which can be calculated using the Wiener-Khintchine theorem that autocorrelation function is the inverse Fourier transform of Power Spectrum Density. Then we can treat  $x[k]$  as a train of randomly

weighted impulses and  $\phi_{xx}[\lambda]$  can be expressed as  $\phi_{xx}[\lambda] = \varepsilon\{x[k + \lambda]x^*[k]\} = \mathcal{F}^{-1}\left\{\frac{\sigma^2}{T}\right\} = \frac{\sigma^2}{T}\delta[k]$ . Then we have

$$\begin{aligned}
\varphi_{dx}[\lambda] &= \varepsilon\{d[k + \lambda]x^*[k]\} \\
&= \varepsilon\left\{\sum_{m=-\infty}^{+\infty} h_{ct}[k + \lambda - m]x[m]x^*[k]\right\} + \varepsilon\{n[k + \lambda]x^*[k]\} \\
&= \sum_{m=-\infty}^{+\infty} h_{ct}[k + \lambda - m] \cdot \varepsilon\{x[m]x^*[k]\} \\
&= \frac{\sigma^2}{T} \sum_{m=-\infty}^{+\infty} h_{ct}[k + \lambda - m] \cdot \delta[m - k] \\
&= \frac{\sigma^2}{T} h_{ct}[\lambda]
\end{aligned}$$

$$\begin{aligned}
\phi_{dd}[\lambda] &= \varepsilon\{d[k + \lambda]d^*[k]\} \\
&= \varepsilon\left\{\sum_{m=-\infty}^{+\infty} \sum_{l=-\infty}^{+\infty} h_{ct}[k + \lambda - m]h_{ct}^*[l]x[m]x^*[k - l]\right\} + \varepsilon\{n[k + \lambda]n^*[k]\} \\
&= \sum_{m=-\infty}^{+\infty} \sum_{l=-\infty}^{+\infty} h_{ct}[k + \lambda - m]h_{ct}^*[l] \cdot \varepsilon\{x[m]x^*[k - l]\} + \frac{N_0}{2}\delta[\lambda] \\
&= \frac{\sigma^2}{T} \sum_{m=-\infty}^{+\infty} \sum_{l=-\infty}^{+\infty} h_{ct}[k + \lambda - m]h_{ct}^*[l] \cdot \delta[m - k + l] + \frac{N_0}{2}\delta[\lambda] \\
&= \frac{\sigma^2}{T} \sum_{l=-\infty}^{+\infty} h_{ct}[l + \lambda]h_{ct}^*[l] + \frac{N_0}{2}\delta[\lambda] \\
&= \frac{\sigma^2}{T} h_{ct}[\lambda] * h_{ct}^*[-\lambda] + \frac{N_0}{2}\delta[\lambda]
\end{aligned}$$

The value of  $\sigma^2$  and  $T$  vary with different modulations. If symbol mean value is 0,  $\sigma^2$  becomes the symbol energy. In section 2.2, the symbol energy of BPSK and QPSK is 1 whereas the symbol energy of 16QAM is 10.  $T$  denotes the time duration of symbols, which depends on the system bandwidth.

## Appendix B.

# Results of KKT Conditions

**Single User Case** Applying the same rules for differentiation in Appendix A, we can have

$$\frac{\partial MSE(g)}{\partial g} = \mathbf{g}^H \widehat{\mathbf{H}} - \mathbf{h}_L$$

Then we have the KKT condition

$$\begin{cases} \mathbf{g}^H \widehat{\mathbf{H}} - \mathbf{h}_L + \lambda \mathbf{h}_L = 0 \\ \mathbf{h}_L \mathbf{g} = 1 \end{cases}$$

From first equation, we can get  $\mathbf{g}^H = (1 - \lambda) \mathbf{h}_L \widehat{\mathbf{H}}^{-1}$ . To get the value of  $\lambda$  we need to combine it with the second equation.

$$\begin{aligned} \mathbf{g}^H \mathbf{h}_L^H &= 1 \\ (1 - \lambda) \mathbf{h}_L \widehat{\mathbf{H}}^{-1} \mathbf{h}_L^H &= 1 \\ (1 - \lambda) &= \frac{1}{\mathbf{h}_L \widehat{\mathbf{H}}^{-1} \mathbf{h}_L^H} \end{aligned}$$

Finally, we have  $\mathbf{g}_{omp} = \frac{\mathbf{h}_L \widehat{\mathbf{H}}^{-1}}{\mathbf{h}_L \widehat{\mathbf{H}}^{-1} \mathbf{h}_L^H}$

**Multiple User Case** The KKT condition of Multiple User Model can be written as

$$\left\{ \begin{array}{l} \mathbf{g}^H \widehat{\mathbf{H}} - \mathbf{h}_L + \sum_{i=1}^N \lambda_i \widehat{\mathbf{h}}_i = 0 \\ \widehat{\mathbf{h}}_1 \mathbf{g} = 1 \\ \vdots \\ \widehat{\mathbf{h}}_N \mathbf{g} = 1 \end{array} \right.$$

From the first equation, we can get  $\mathbf{g}^H = \sum_{i=1}^N \lambda_i \widehat{\mathbf{h}}_i \widehat{\mathbf{H}}^{-1}$ . Here, we replace  $1 - \lambda_i$  by  $\lambda_i$  for easier computation. Then, combine it with other equations. The resulting equations are listed below:

$$\left\{ \begin{array}{l} \lambda_1 \widehat{\mathbf{h}}_1 \widehat{\mathbf{H}}^{-1} \widehat{\mathbf{h}}_1^H + \lambda_2 \widehat{\mathbf{h}}_2 \widehat{\mathbf{H}}^{-1} \widehat{\mathbf{h}}_1^H + \cdots + \lambda_N \widehat{\mathbf{h}}_N \widehat{\mathbf{H}}^{-1} \widehat{\mathbf{h}}_1^H = 1 \\ \lambda_1 \widehat{\mathbf{h}}_1 \widehat{\mathbf{H}}^{-1} \widehat{\mathbf{h}}_2^H + \lambda_2 \widehat{\mathbf{h}}_2 \widehat{\mathbf{H}}^{-1} \widehat{\mathbf{h}}_2^H + \cdots + \lambda_N \widehat{\mathbf{h}}_N \widehat{\mathbf{H}}^{-1} \widehat{\mathbf{h}}_2^H = 1 \\ \vdots \\ \lambda_1 \widehat{\mathbf{h}}_1 \widehat{\mathbf{H}}^{-1} \widehat{\mathbf{h}}_N^H + \lambda_2 \widehat{\mathbf{h}}_2 \widehat{\mathbf{H}}^{-1} \widehat{\mathbf{h}}_N^H + \cdots + \lambda_N \widehat{\mathbf{h}}_N \widehat{\mathbf{H}}^{-1} \widehat{\mathbf{h}}_N^H = 1 \end{array} \right.$$

Then, write it in vector form, we have

$$\begin{bmatrix} \widehat{\mathbf{h}}_1 \widehat{\mathbf{H}}^{-1} \widehat{\mathbf{h}}_1^H & \widehat{\mathbf{h}}_2 \widehat{\mathbf{H}}^{-1} \widehat{\mathbf{h}}_1^H & \cdots & \widehat{\mathbf{h}}_N \widehat{\mathbf{H}}^{-1} \widehat{\mathbf{h}}_1^H \\ \widehat{\mathbf{h}}_1 \widehat{\mathbf{H}}^{-1} \widehat{\mathbf{h}}_2^H & \widehat{\mathbf{h}}_2 \widehat{\mathbf{H}}^{-1} \widehat{\mathbf{h}}_2^H & \cdots & \widehat{\mathbf{h}}_N \widehat{\mathbf{H}}^{-1} \widehat{\mathbf{h}}_2^H \\ \vdots & \vdots & \ddots & \vdots \\ \widehat{\mathbf{h}}_1 \widehat{\mathbf{H}}^{-1} \widehat{\mathbf{h}}_N^H & \widehat{\mathbf{h}}_2 \widehat{\mathbf{H}}^{-1} \widehat{\mathbf{h}}_N^H & \cdots & \widehat{\mathbf{h}}_N \widehat{\mathbf{H}}^{-1} \widehat{\mathbf{h}}_N^H \end{bmatrix} \begin{bmatrix} \lambda_1 \\ \lambda_2 \\ \vdots \\ \lambda_N \end{bmatrix} = \begin{bmatrix} 1 \\ 1 \\ \vdots \\ 1 \end{bmatrix}$$

Then we have

$$\boldsymbol{\lambda} = \boldsymbol{\Omega}^{-1} \mathbf{I}$$

# Bibliography

- [1] Y. Chen, F. Han, Y.-H. Yang, H. Ma, Y. Han, C. Jiang, H.-Q. Lai, D. Claffey, Z. Safar, and K. R. Liu, “Time-reversal wireless paradigm for green internet of things: An overview,” *IEEE Internet of Things Journal*, vol. 1, no. 1, pp. 81–98, 2014.
- [2] Y. Chen, Y.-H. Yang, F. Han, and K. R. Liu, “Time-reversal wideband communications,” *IEEE Signal Processing Letters*, vol. 20, no. 12, pp. 1219–1222, 2013.
- [3] R. C. Qiu, C. Zhou, N. Guo, and J. Q. Zhang, “Time reversal with miso for ultrawideband communications: Experimental results,” *IEEE Antennas and Wireless Propagation Letters*, vol. 5, no. 1, pp. 269–273, Dec 2006.
- [4] B. Wang, Y. Wu, F. Han, Y.-H. Yang, and K. R. Liu, “Green wireless communications: A time-reversal paradigm,” *IEEE Journal on Selected Areas in Communications*, vol. 29, no. 8, pp. 1698–1710, 2011.
- [5] M. Fink, C. Prada, F. Wu, and D. Cassereau, “Self focusing in inhomogeneous media with time reversal acoustic mirrors,” in *Proceedings., IEEE Ultrasonics Symposium*, Oct 1989, pp. 681–686 vol.2.
- [6] M. Fink, “Time reversal of ultrasonic fields. i. basic principles,” *IEEE Transactions on Ultrasonics, Ferroelectrics, and Frequency Control*, vol. 39, no. 5, pp. 555–566, Sept 1992.
- [7] A. Derode, P. Roux, and M. Fink, “Acoustic time-reversal through high-order multiple scattering,” in *1995 IEEE Ultrasonics Symposium. Proceedings. An International Symposium*, vol. 2, Nov 1995, pp. 1091–1094 vol.2.
- [8] W. A. Kuperman, W. S. Hodgkiss, H. C. Song, T. Akal, C. Ferla, and D. R. Jackson, “Phase conjugation in the ocean: Experimental demonstration of an acoustic time-reversal mirror,” *Journal of the Acoustical Society of America*, vol. 103, no. 1, pp. 25–40, Jan 1998, n/a. [Online]. Available: [⟨GotoISI⟩://WOS:000071496900002](http://GotoISI://WOS:000071496900002)
- [9] G. F. Edelmann, T. Akal, W. S. Hodgkiss, S. Kim, W. A. Kuperman, and H. C. Song, “An initial demonstration of underwater acoustic communication using time reversal,” *IEEE Journal of Oceanic Engineering*, vol. 27, no. 3, pp. 602–609, Jul 2002.
- [10] G. Lerosey, J. De Rosny, A. Tourin, A. Derode, G. Montaldo, and M. Fink, “Time reversal of electromagnetic waves,” *Physical review letters*, vol. 92, no. 19, p. 193904, 2004.
- [11] B. E. Henty and D. D. Stancil, “Multipath-enabled super-resolution for rf and microwave communication using phase-conjugate arrays,” *Physical Review Letters*, vol. 93, no. 24, p. 243904, Dec. 2004.
- [12] G. Lerosey, J. d. Rosny, A. Tourin, A. Derode, G. Montaldo, and M. Fink, “Time reversal of electromagnetic waves and telecommunication,” *Radio Science*, vol. 40, no. 06, pp. 1–10, Dec 2005.
- [13] J. de Rosny, G. Lerosey, and M. Fink, “Theory of electromagnetic time-reversal mirrors,” *IEEE Transactions on Antennas and Propagation*, vol. 58, no. 10, pp. 3139–3149, Oct 2010.
- [14] P. Blomgren, P. Kyritsi, A. D. Kim, and G. Papanicolaou, “Spatial focusing and intersymbol interference in multiple-input single-output time reversal communication systems,” *IEEE Journal of Oceanic Engineering*, vol. 33, no. 3, pp. 341–355, July 2008.
- [15] G. Montaldo, G. Lerosey, A. Derode, A. Tourin, J. de Rosny, and M. Fink, “Telecommunication in a disordered environment with iterative time reversal,” *The Journal of the Acoustical Society of America*, vol. 117, no. 4, pp. 2560–2561, 2005. [Online]. Available: <http://dx.doi.org/10.1121/1.4788522>

- [16] H. T. Nguyen, I. Z. Kovcs, and P. C. F. Eggers, “A time reversal transmission approach for multiuser uwb communications,” *IEEE Transactions on Antennas and Propagation*, vol. 54, no. 11, pp. 3216–3224, Nov 2006.
- [17] F. Han, Y. H. Yang, B. Wang, Y. Wu, and K. J. R. Liu, “Time-reversal division multiple access over multi-path channels,” *IEEE Transactions on Communications*, vol. 60, no. 7, pp. 1953–1965, July 2012.
- [18] Q. Xu, Y. Chen, and K. J. R. Liu, “Optimal pricing for interference control in time-reversal device-to-device uplinks,” in *2015 IEEE Global Conference on Signal and Information Processing (GlobalSIP)*, Dec 2015, pp. 1096–1100.
- [19] Y. H. Yang and K. J. R. Liu, “Waveform design with interference pre-cancellation beyond time-reversal systems,” *IEEE Transactions on Wireless Communications*, vol. 15, no. 5, pp. 3643–3654, May 2016.
- [20] A. F. Molisch, K. Balakrishnan, C.-C. Chong, S. Emami, A. Fort, J. Karedal, J. Kunisch, H. Schantz, U. Schuster, and K. Siwiak, “Ieee 802.15. 4a channel model-final report,” *IEEE P802*, vol. 15, no. 04, p. 0662, 2004.
- [21] A. A. Saleh and R. Valenzuela, “A statistical model for indoor multipath propagation,” *IEEE Journal on selected areas in communications*, vol. 5, no. 2, pp. 128–137, 1987.
- [22] M. Emami, M. Vu, J. Hansen, A. J. Paulraj, and G. Papanicolaou, “Matched filtering with rate back-off for low complexity communications in very large delay spread channels,” in *Signals, Systems and Computers, 2004. Conference Record of the Thirty-Eighth Asilomar Conference on*, vol. 1. IEEE, 2004, pp. 218–222.